

The structure of mode-locking regions of piecewise-linear continuous maps: II. Skew sawtooth maps.

D.J.W. Simpson

Institute of Fundamental Sciences
Massey University
Palmerston North
New Zealand

December 14, 2016

Abstract

In two-parameter bifurcation diagrams of piecewise-linear continuous maps on \mathbb{R}^N , mode-locking regions typically have points of zero width known as shrinking points. Near any shrinking point, but outside the associated mode-locking region, a significant proportion of parameter space can be usefully partitioned into a two-dimensional array of nearly-hyperbolic annular sectors. The purpose of this paper is to show that in these sectors the dynamics is well-approximated by a three-parameter family of skew sawtooth circle maps, where the relationship between the skew sawtooth maps and the N -dimensional map is fixed within each sector. The skew sawtooth maps are continuous, degree-one, and piecewise-linear, with two different slopes. They approximate the stable dynamics of the N -dimensional map with an error that goes to zero with the distance from the shrinking point. The results explain the complicated radial pattern of periodic, quasi-periodic, and chaotic dynamics that occurs near shrinking points.

1 Introduction

This paper extends the study of [1] for piecewise-linear maps on \mathbb{R}^N ($N \geq 2$) that are continuous and involve two pieces. For such maps, coordinates $x \in \mathbb{R}^N$ can be chosen such that the hyperplane along which the two pieces are joined, termed the switching manifold, is simply where the first coordinate of x vanishes. Using s to denote the first coordinate of x , i.e.

$$s := e_1^\top x, \quad (1.1)$$

such a map takes the form

$$x_{i+1} = f(x_i; \xi) := \begin{cases} A_L(\xi)x_i + B(\xi), & s_i \leq 0, \\ A_R(\xi)x_i + B(\xi), & s_i \geq 0, \end{cases} \quad (1.2)$$

where A_L and A_R are real-valued $N \times N$ matrices and $B \in \mathbb{R}^N$. It is assumed that A_L , A_R , and B have a C^K ($K \geq 2$) dependency on a parameter $\xi \in \mathbb{R}^M$ ($M \geq 2$). The assumption that f is continuous on $s = 0$ implies $A_R = A_L + Ce_1^T$ for some $C \in \mathbb{R}^N$.

Maps of the form (1.2) describe the dynamics near border-collision bifurcations of piecewise-smooth maps [2, 3]. Piecewise-smooth maps arise as return maps for nonsmooth differential equations which serve as useful mathematical models of phenomena with events that are discontinuous or at least fast relative to the usual motion of the system. Examples of such systems exhibiting border-collision bifurcations include neurons with square wave forcing [4], mechanical oscillators with friction [5, 6], and DC/DC power converters [7, 8]. Maps of the form (1.2) also arise as models of discrete-time phenomena involving a switching element, such as trade cycle models with non-negativity constraints [9].

To illustrate the ideas of this paper, consider

$$A_L = \begin{bmatrix} \tau_L & 1 & 0 \\ -\sigma_L & 0 & 1 \\ \delta_L & 0 & 0 \end{bmatrix}, \quad A_R = \begin{bmatrix} \tau_R & 1 & 0 \\ -\sigma_R & 0 & 1 \\ \delta_R & 0 & 0 \end{bmatrix}, \quad B = \begin{bmatrix} \mu \\ 0 \\ 0 \end{bmatrix}, \quad (1.3)$$

where $\xi = (\tau_L, \sigma_L, \delta_L, \tau_R, \sigma_R, \delta_R, \mu) \in \mathbb{R}^7$. The map (1.2) with (1.3) is the border-collision normal form in three dimensions [10]. Fig. 1 shows mode-locking regions of (1.2) with (1.3) and

$$\tau_L = 0, \quad \sigma_L = -1, \quad \sigma_R = 0, \quad \delta_R = 2, \quad \mu = 1. \quad (1.4)$$

Each coloured region is a mode-locking region where (1.2) has an attracting periodic solution of a fixed rotation number. The regions are roughly ordered by rotation number and are more narrow for higher periods.

Unlike mode-locking regions of smooth maps, the mode-locking regions in Fig. 1 have points of zero width. These are termed shrinking points and have been described in a wide variety of mathematical models that can be put in the form (1.2), or are at least well-approximated by a map of form (1.2), see for instance [4, 11, 12, 13, 14]. In a mode-locking region, as we cross a shrinking point the number of points that the corresponding periodic solution has on each side of the switching manifold changes by one. In a neighbourhood of a shrinking point, the mode-locking region is bounded by four curves along which an \mathcal{S} -cycle (periodic solution with symbolic itinerary $\mathcal{S} \in \{L, R\}^{\mathbb{Z}}$) has one point on the switching manifold for a particular sequence \mathcal{S} [15], and the shrinking point is referred to as an \mathcal{S} -shrinking point.

Now consider the dynamics near an \mathcal{S} -shrinking point but outside its corresponding mode-locking region. Let $\frac{m}{n}$ be the rotation number associated with \mathcal{S} . As explained in [1], the most dominant nearby mode-locking regions have rotation numbers $\frac{m_k^-}{n_k^-} = \frac{km+m^-}{kn+n^-}$ and $\frac{m_k^+}{n_k^+} = \frac{km+m^+}{kn+n^+}$, where $k \in \mathbb{Z}^+$ and $\frac{m^-}{n^-}$ and $\frac{m^+}{n^+}$ are the left and right Farey roots of $\frac{m}{n}$. These regions, termed \mathcal{G}_k^\pm -mode-locking regions, form two sequences that approach the \mathcal{S} -shrinking point from opposite sides as $k \rightarrow \infty$. The existence and location of shrinking points on the \mathcal{G}_k^\pm -mode-locking regions is determined by various scalar quantities associated with the \mathcal{S} -shrinking point.

The results in [1] were obtained by performing calculations on one-dimensional centre manifolds. This paper concerns circle maps that capture an approximate return to a fundamental domain of such a manifold. The maps are continuous, piecewise-linear, and degree-one. They

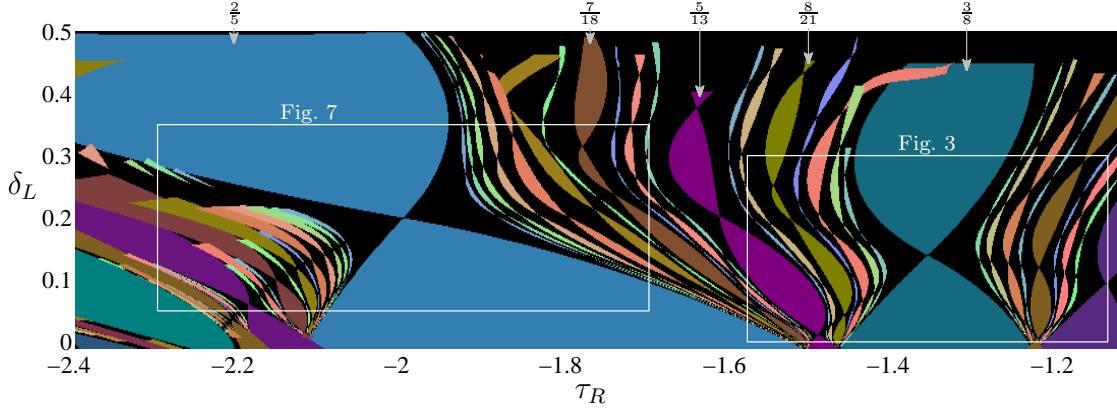


Figure 1: Mode-locking regions of (1.2)–(1.4). Only mode-locking regions corresponding to rotational periodic solutions (defined in §2.2) are shown as other mode-locking regions are relatively small, do not exhibit shrinking points, and require more computation time to obtain to the same degree of accuracy. This figure was computed by numerically checking the existence and stability of rotational periodic solutions up to period 50 on a 1024×256 grid of τ_R and δ_L values. At grid points where mode-locking regions overlap, the solution of the highest period is indicated. Five of the mode-locking regions are labelled by their rotation number.

are written as

$$z_{i+1} = g(z_i; a_L, a_R, w) := \begin{cases} (w + a_L(z_i - z_{\text{sw}}) + z_{\text{sw}}) \bmod 1, & 0 \leq z_i \leq z_{\text{sw}}, \\ (w + a_R(z_i - z_{\text{sw}}) + z_{\text{sw}}) \bmod 1, & z_{\text{sw}} \leq z_i < 1, \end{cases} \quad (1.5)$$

where $z \in [0, 1)$ is the state variable,

$$a_L < 1, \quad a_R > 1, \quad w \in \mathbb{R}, \quad (1.6)$$

are parameters, and

$$z_{\text{sw}} := \frac{a_R - 1}{a_R - a_L}. \quad (1.7)$$

As shown in Fig. 2, a_L and a_R are the slopes of (1.5) and w is the vertical displacement (modulo 1) of (1.5) at the kink $z = z_{\text{sw}}$. Equation (1.5) is termed a *skew sawtooth map* because with $a_L + a_R = 2$ (giving $z_{\text{sw}} = \frac{1}{2}$) it is commonly known as a sawtooth map [16]. As a three-parameter family, (1.5) is equivalent to the “tip maps” studied in [17].

Here it is briefly shown how (1.5) can be used to approximate the dynamics of (1.2) near shrinking points, with details to be provided in later sections. In a neighbourhood of an \mathcal{S} -shrinking point, the inner boundaries of the \mathcal{G}_k^\pm -mode-locking regions are used to define a grid of sectors $\Sigma_{k, \Delta\ell}^\pm$, where $\Delta\ell \in \mathbb{Z}$. As an example, Fig. 3 shows a magnification of Fig. 1 centred at the \mathcal{S} -shrinking point with $\mathcal{S} = LRRLRRLR$. Here \mathcal{G}_k^\pm -mode-locking regions are shaded dark grey and all other nearby mode-locking regions are shaded light grey. Fig. 3 also shows two representative sectors, $\Sigma_{2,0}^+$ and $\Sigma_{3,1}^+$, and indicates the dynamics of (1.2) in these sectors. Fig. 4 shows the approximate location of the sectors $\Sigma_{k, \Delta\ell}^\pm$ for Fig. 3 as given by truncating an asymptotic expansion in powers of $\frac{1}{k}$ to leading order.

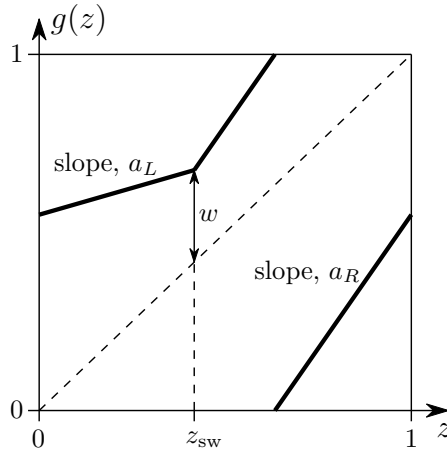


Figure 2: A sketch of the skew sawtooth map (1.5).

Within each $\Sigma_{k,\Delta\ell}^\pm$, $\delta \geq 0$ measures the distance to the outer boundary of $\Sigma_{k,\Delta\ell}^\pm$ in a radial direction and $\theta \in [0, 2\pi)$ measures the angle about the \mathcal{S} -shrinking point. In (δ, θ) -coordinates the sectors are rectangular in the approximation of Fig. 4:

$$\Sigma_{k,\Delta\ell}^\pm \approx \left\{ (\delta, \theta) \mid 0 \leq \delta \leq \frac{1}{k^2}, \theta_{\min} \leq \theta \leq \theta_{\max} \right\}, \quad (1.8)$$

where $\theta_{\min}, \theta_{\max} \in [0, 2\pi)$ depend only on the value of $\Delta\ell$.

For $\Sigma_{2,0}^+$ and $\Sigma_{3,1}^+$, Fig. 5 shows mode-locking regions of (1.5) using

$$a_L = \frac{\tan(\theta)}{\tan(\theta_{\min})}, \quad a_R = \frac{\tan(\theta)}{\tan(\theta_{\max})}, \quad w = k^2 \delta. \quad (1.9)$$

Equation (1.9) represents the appropriate transformation from (δ, θ) -coordinates to the parameter space of (1.5) for $\Sigma_{2,0}^+$ and $\Sigma_{3,1}^+$. By comparing Figs. 3 and 5, it is evident that the dynamics of (1.2) in $\Sigma_{2,0}^+$ and $\Sigma_{3,1}^+$ matches well to that of (1.5) using (1.9). Moreover, the dynamics of (1.2) in each $\Sigma_{k,0}^+$ and $\Sigma_{k,1}^+$ matches that of (1.5) using (1.9) with an error of order $\mathcal{O}(\frac{1}{k})$ and where one iterate of (1.5) corresponds to roughly kn iterates of (1.2) (here $n = 8$).

The remainder of this paper is organised as follows. In §2, the sectors $\Sigma_{k,\Delta\ell}^\pm$ and (δ, θ) -coordinates are defined more precisely. The correspondence between (1.2) and (1.5) is clarified and used to explain the bifurcation structure of (1.2) near a typical shrinking point. In §3 some important identities for the symbolic itineraries of periodic solutions in \mathcal{G}^\pm -mode-locking regions are derived and an attracting one-dimensional centre manifold W^c and a fundamental domain $\Omega_{\Delta\ell} \subset W^c$ are introduced.

In §4, $\Omega_{\Delta\ell}$ is enlarged into an N -dimensional set Φ that forward orbits of (1.2) regularly visit. The set Φ is interpreted as a cylinder and topological arguments are used to prove that the first return map $F : \Phi \rightarrow \Phi$ has an attracting invariant set that is homotopic to $\Omega_{\Delta\ell}$. This shows that (1.2) has an attracting invariant set homotopic to a circle on which the dynamics is well approximated by (1.5). In §5 the necessary calculations to achieve this approximation are performed, with the main result given by Theorem 5.2. Finally §6 provides concluding remarks.

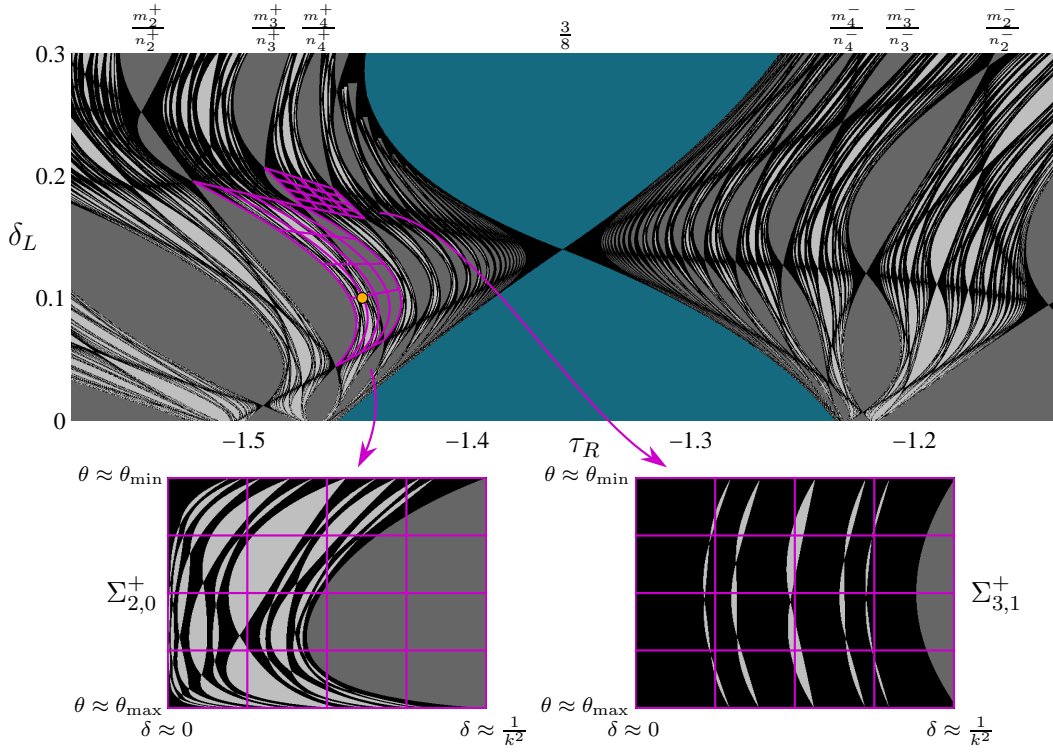


Figure 3: Mode-locking regions of (1.2)–(1.4) centred about the \mathcal{S} -shrinking point of Fig. 1 with $\mathcal{S} = \mathcal{F}[3, 3, 8] = LRRLRRLR$ (here $\frac{m}{n} = \frac{3}{8}$). In order to show many mode-locking regions (up to period 150), the mode-locking regions were approximated by detecting periodicity, within some tolerance, of the forward orbit of $x = (0, 0, 0)$ computed for 10^5 iterates over a 2048×512 grid of τ_R and δ_L values. The rotation numbers $\frac{m_k^-}{n_k^-}$ and $\frac{m_k^+}{n_k^+}$ are given by (2.17) where here $\frac{m^-}{n^-} = \frac{1}{3}$ and $\frac{m^+}{n^+} = \frac{2}{5}$ are the left and right Farey roots of $\frac{m}{n} = \frac{3}{8}$. The sectors $\Sigma_{2,0}^+$ and $\Sigma_{3,1}^+$ are also shown. To four decimal places, these admit the approximation (1.8) with $\theta_{\min} = 5.1288$ and $\theta_{\max} = 6.1315$ for $\Sigma_{2,0}^+$, and $\theta_{\min} = 4.9844$ and $\theta_{\max} = 5.1288$ for $\Sigma_{3,1}^+$. The coloured dot in $\Sigma_{2,0}^+$ indicates the parameter values of Fig. 11-A.

Throughout this paper, but mostly in proofs, particular places in [1] are referenced. Some proofs are deferred to Appendix A and some formulas of [1] are given in Appendix B. For brevity, Sections 3–5 only provide calculations for sectors $\Sigma_{k,\Delta\ell}^+$ with $\Delta\ell \geq 0$.

2 Main results

In this section we first describe periodic solutions of (1.2), §2.1. We then discuss shrinking points and briefly review the notation of [1] in §2.2. In §2.3 we describe \mathcal{G}_k^\pm -mode-locking regions and in §2.4 define the sectors $\Sigma_{k,\Delta\ell}^\pm$. We then detail the correspondence between (1.2) and (1.5) in §2.5 and finally use this to explain the dynamics of (1.2) near a typical shrinking point in §2.6.

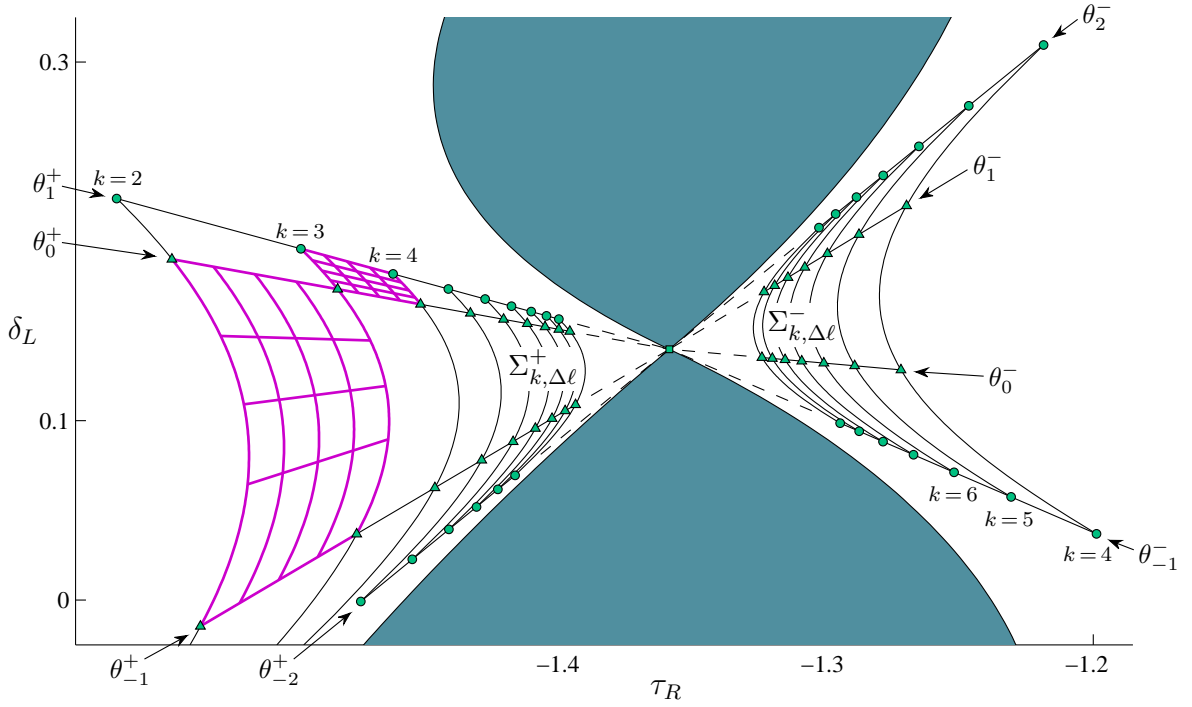


Figure 4: The leading order approximation to the location of the sectors $\Sigma_{k, \Delta \ell}^\pm$ for the example shown in Fig. 3. To four decimal places: $\theta_{-1}^- = 1.6222$, $\theta_0^- = 2.1401$, $\theta_1^- = 3.0002$, $\theta_2^- = 3.1268$, $\theta_1^+ = 4.9844$, $\theta_0^+ = 5.1288$, $\theta_{-1}^+ = 6.1315$, $\theta_{-2}^+ = 6.2705$. These values provide the bounds for (1.8).

2.1 Periodic solutions

We denote the two components of (1.2) by

$$f^L(x; \xi) := A_L(\xi)x + B(\xi), \quad f^R(x; \xi) := A_R(\xi)x + B(\xi). \quad (2.1)$$

Given a periodic symbol sequence $\mathcal{S} \in \{L, R\}^{\mathbb{Z}}$ of period n , we let

$$f^{\mathcal{S}} := f^{\mathcal{S}_{n-1}} \circ \dots \circ f^{\mathcal{S}_0}, \quad (2.2)$$

denote the composition of f^L and f^R in the order specified by \mathcal{S} . The map $f^{\mathcal{S}}$ is given by

$$f^{\mathcal{S}}(x) = M_{\mathcal{S}}x + P_{\mathcal{S}}B, \quad (2.3)$$

where

$$M_{\mathcal{S}} := A_{\mathcal{S}_{n-1}} \cdots A_{\mathcal{S}_0}, \quad (2.4)$$

$$P_{\mathcal{S}} := I + A_{\mathcal{S}_{n-1}} + A_{\mathcal{S}_{n-1}}A_{\mathcal{S}_{n-2}} + \cdots + A_{\mathcal{S}_{n-1}} \cdots A_{\mathcal{S}_1}. \quad (2.5)$$

An \mathcal{S} -cycle is defined as an n -tuple, $\{x_i^{\mathcal{S}}\}_{i=0}^{n-1}$ for which

$$f^{\mathcal{S}_0}(x_0^{\mathcal{S}}) = x_1^{\mathcal{S}}, \quad f^{\mathcal{S}_1}(x_1^{\mathcal{S}}) = x_2^{\mathcal{S}}, \quad \dots, \quad f^{\mathcal{S}_{n-1}}(x_{n-1}^{\mathcal{S}}) = x_0^{\mathcal{S}}. \quad (2.6)$$

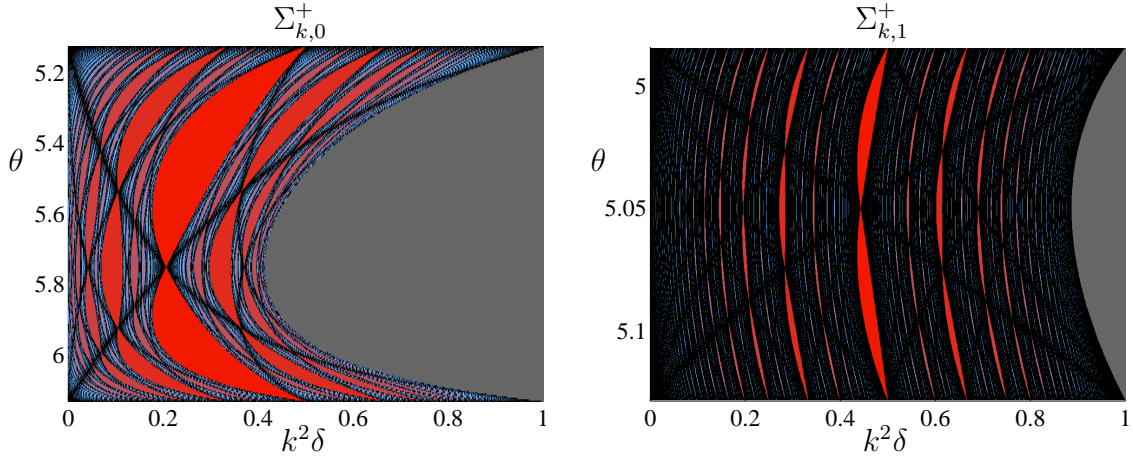


Figure 5: Mode-locking regions of (1.5) with (1.9) corresponding to $\Sigma_{k,0}^+$ and $\Sigma_{k,1}^+$ of Fig. 3, where $k \in \mathbb{Z}^+$. In both plots the rotation number (with respect to (1.5)) associated with each mode-locking region is equal to its value of $w = k^2\delta$ at both the top of the figure (where $a_L = 1$) and the bottom of the figure (where $a_R = 1$). To four decimal places, $\frac{a_R}{a_L} = 14.7884$ for $\Sigma_{k,0}^+$, and $\frac{a_R}{a_L} = 1.5856$ for $\Sigma_{k,1}^+$. Note, the θ -axis is reversed to match Fig. 3.

If $s_i^S \leq 0$ for every i for which $\mathcal{S}_i = L$, and $s_i^S \geq 0$ for every i for which $\mathcal{S}_i = R$, then each point x_i^S lies on the side of the switching manifold corresponding to \mathcal{S}_i . In this case the \mathcal{S} -cycle is a periodic solution of f and we say it is *admissible*. If it is not admissible we say it is *virtual*.

Each point x_i^S is a fixed point of $f^{\mathcal{S}^{(i)}}$, where $\mathcal{S}^{(i)}$ denotes the i^{th} left shift permutation of \mathcal{S} (i.e. $\mathcal{S}_j^{(i)} = \mathcal{S}_{i+j}$, for all $j \in \mathbb{Z}$). If $\det(I - M_{\mathcal{S}}) \neq 0$, then x_i^S is unique and given by

$$x_i^S = (I - M_{\mathcal{S}^{(i)}})^{-1} P_{\mathcal{S}^{(i)}} B. \quad (2.7)$$

Given $\ell, m, n \in \mathbb{Z}^+$, with $\ell < n$, $m < n$ and $\gcd(m, n) = 1$, we define a symbol sequence $\mathcal{F}[\ell, m, n] \in \{L, R\}^{\mathbb{Z}}$ by

$$\mathcal{F}[\ell, m, n]_i := \begin{cases} L, & im \bmod n < \ell, \\ R, & im \bmod n \geq \ell. \end{cases} \quad (2.8)$$

Each $\mathcal{F}[\ell, m, n]$ describes the action of stepping through n points on a circle, ℓ of which lie to the left of the switching manifold, with rotation number $\frac{m}{n}$, [15, 18]. Indeed, we call $\frac{m}{n}$ the *rotation number* of $\mathcal{F}[\ell, m, n]$, and refer to such symbol sequences and their shift permutations as *rotational*. Rotational symbol sequences satisfy the important identity

$$\mathcal{F}[\ell, m, n]^{\bar{0}\bar{\ell}\bar{d}} = \mathcal{F}[\ell, m, n]^{(-d)}, \quad (2.9)$$

where d denotes the multiplicative inverse of m modulo n , and we use the notation $\mathcal{S}^{\bar{i}}$ to denote the symbol sequence that differs from \mathcal{S} in only the indices $i + jn$, for all $j \in \mathbb{Z}$.

2.2 Shrinking points

We use rotational symbol sequences to define shrinking points of (1.2). Let $\mathcal{S} = \mathcal{F}[\ell, m, n]$ be a rotational symbol sequence with $2 \leq \ell \leq n - 2$. Suppose that at some point in parameter space

ξ , the following three genericity conditions are satisfied:

$$e_1^\top \text{adj}(I - A_L) B \neq 0, \quad \det(I - M_{\mathcal{S}\bar{\sigma}}) \neq 0, \quad \det(I - M_{\mathcal{S}\bar{\tau}}) \neq 0. \quad (2.10)$$

In view of the second condition, the \mathcal{S}^σ -cycle is unique. If the \mathcal{S}^σ -cycle is also admissible, with $s_i^{\mathcal{S}^\sigma} = 0$ if and only if $i = 0$ or $i = \ell d \bmod n$, then we say that ξ is an \mathcal{S} -shrinking point.

As in [1], at an \mathcal{S} -shrinking point we let

$$a := \det(I - M_{\mathcal{S}\bar{\sigma}}), \quad b := \det(I - M_{\mathcal{S}\bar{\tau}}), \quad (2.11)$$

and

$$y_i := x_i^{\mathcal{S}^\sigma}, \quad t_i := s_i^{\mathcal{S}^\sigma}, \quad (2.12)$$

for each i . Many identities involving quantities associated with an \mathcal{S} -shrinking point, such as (2.11)–(2.12), are given in [1]. Of these, perhaps the most fundamental is

$$\frac{a}{b} = -\frac{t_d t_{(\ell-1)d}}{t_{-d} t_{(\ell+1)d}}, \quad (2.13)$$

which was first given in [19].

By Lemma 5.8 of [1], at an \mathcal{S} -shrinking point 0 is an eigenvalue of $M_{\mathcal{S}}$ with multiplicity one. We let

$$\rho_{\max} := \max_{j=2, \dots, N} |\rho_j|, \quad (2.14)$$

where ρ_j are the eigenvalues of $M_{\mathcal{S}}$, counting multiplicity, with $\rho_1 = 1$, and

$$c := \prod_{j=2}^N (1 - \rho_j). \quad (2.15)$$

If $\rho_{\max} < 1$ then \mathcal{S} -cycles are stable for some parameter values near the \mathcal{S} -shrinking point ensuring that the \mathcal{S} -shrinking point is connected to part of a mode-locking region involving \mathcal{S} -cycles (instead of merely a periodicity region involving only unstable \mathcal{S} -cycles). Note that $\rho_{\max} < 1$ implies $c > 0$ (Lemma 7.4 of [1]).

2.3 \mathcal{G}_k^\pm -mode-locking regions

Let $\mathcal{F}[\ell, m, n]$ be a rotational symbol sequence. Let $\frac{m^-}{n^-}$ and $\frac{m^+}{n^+}$ denote the left and right Farey roots of $\frac{m}{n}$, and let $\ell^- := \left\lfloor \frac{\ell n^-}{n} \right\rfloor$ and $\ell^+ := \left\lceil \frac{\ell n^+}{n} \right\rceil$. Let $k \in \mathbb{Z}^+$ and $\Delta \ell \in \mathbb{Z}$ with $|\Delta \ell| < k$. We then define

$$\mathcal{G}^\pm[k, \Delta \ell] := \mathcal{F}[\ell_k^\pm + \Delta \ell, m_k^\pm, n_k^\pm], \quad (2.16)$$

where

$$\ell_k^\pm := k\ell + \ell^\pm, \quad m_k^\pm := km + m^\pm, \quad n_k^\pm := kn + n^\pm. \quad (2.17)$$

We also let d_k^\pm denote the multiplicative inverse of m_k^\pm modulo n_k^\pm . The rotation number of $\mathcal{G}^\pm[k, \Delta \ell]$ is $\frac{m_k^\pm}{n_k^\pm}$. These rotation numbers represent the first level of complexity relative to $\frac{m}{n}$

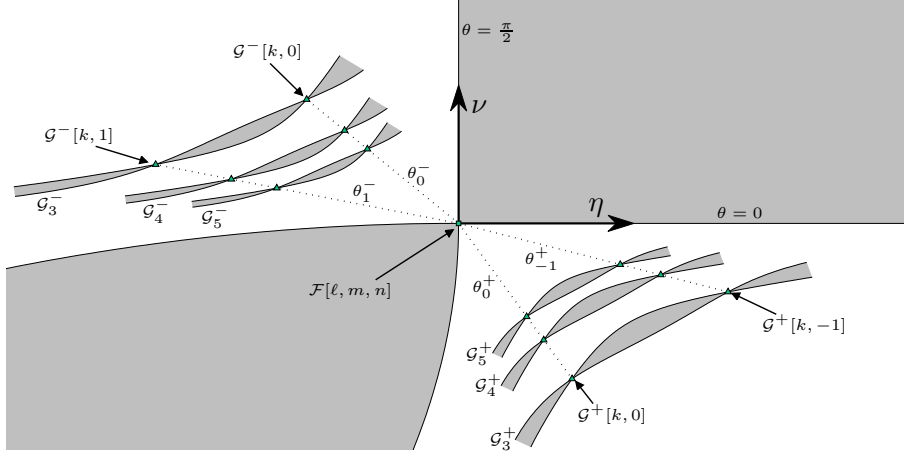


Figure 6: A sketch of typical \mathcal{G}_k^\pm -mode-locking regions in (η, ν) -coordinates in the case $a < 0$. (Taken from [1].)

[20]. As mentioned in §1, we refer to a mode-locking region with rotation number $\frac{m_k^\pm}{n_k^\pm}$ as a \mathcal{G}_k^\pm -mode-locking region.

For simplicity we assume $\xi \in \mathbb{R}^2$ and write $\xi = (\xi_1, \xi_2)$. In a neighbourhood of an \mathcal{S} -shrinking point, where $\mathcal{S} = \mathcal{F}[\ell, m, n]$, let

$$\eta := s_0^{\mathcal{S}\bar{0}}(\xi_1, \xi_2), \quad \nu := s_{\ell d}^{\mathcal{S}\bar{0}}(\xi_1, \xi_2). \quad (2.18)$$

Throughout this paper we assume that $(\xi_1, \xi_2) \rightarrow (\eta, \nu)$ is a locally invertible coordinate change. That is, $\det(J) \neq 0$, where $J := \begin{bmatrix} \frac{\partial \eta}{\partial \xi_1} & \frac{\partial \eta}{\partial \xi_2} \\ \frac{\partial \nu}{\partial \xi_1} & \frac{\partial \nu}{\partial \xi_2} \end{bmatrix}$ evaluated at the shrinking point. We have $s_0^{\mathcal{S}\bar{0}} = s_{\ell d}^{\mathcal{S}\bar{0}} = 0$ at the \mathcal{S} -shrinking point. Thus in (η, ν) -coordinates the \mathcal{S} -shrinking point is located at the origin.

As in [1], we define polar coordinates (r, θ) by

$$\eta = \left| \frac{ct_d}{a} \right| r \cos(\theta), \quad \nu = \left| \frac{ct_{(\ell-1)d}}{a} \right| r \sin(\theta), \quad (2.19)$$

where a , c , t_d and $t_{(\ell-1)d}$ are defined by (2.11)–(2.12). If $a < 0$, then \mathcal{G}_k^+ -mode-locking regions exist for $\theta \in (\frac{3\pi}{2}, 2\pi)$ and \mathcal{G}_k^- -mode-locking regions exist for $\theta \in (\frac{\pi}{2}, \pi)$, see Fig. 6. If $a > 0$, then the opposite is true.

For large values of k , the \mathcal{G}_k^\pm -mode-locking regions are narrow regions that lie within $\mathcal{O}(\frac{1}{k^2})$ of the curve

$$r = \frac{1}{k} \Gamma(\theta), \quad (2.20)$$

where Γ is defined by

$$\Gamma(\theta) := \begin{cases} \frac{\ln(\cos(\theta)) - \ln(\sin(\theta))}{\cos(\theta) - \sin(\theta)}, & \theta \in (0, \frac{\pi}{2}) \setminus \{\frac{\pi}{4}\}, \\ \sqrt{2}, & \theta = \frac{\pi}{4}, \end{cases} \quad (2.21)$$

for $\theta \in (0, \frac{\pi}{2})$, and defined by $\Gamma(\theta) = \Gamma(\theta \bmod \frac{\pi}{2})$ for all other non-integer multiples of $\frac{\pi}{2}$.

The existence of shrinking points on the \mathcal{G}_k^\pm -mode-locking regions for large values of k is determined by scalar quantities $\kappa_{\Delta\ell}^\pm$ that are associated with the \mathcal{S} -shrinking point. Formulas for these are given in Appendix B. If $\rho_{\max} < 1$ and certain admissibility conditions are satisfied, then given $\Delta\ell \in \mathbb{Z}$ and a choice of $+$ or $-$, \mathcal{G}_k^\pm -mode-locking regions have $\mathcal{G}^\pm[k, \Delta\ell]$ -shrinking points for all sufficiently large values of k if $\kappa_{\Delta\ell}^\pm > 0$, see Theorem 2.2 of [1]. If instead $\kappa_{\Delta\ell}^\pm < 0$, then the mode-locking regions have short stability-loss boundaries where the $\mathcal{G}^\pm[k, \Delta\ell]$ -cycle has a stability multiplier of -1 .

To leading order, the θ -values of the $\mathcal{G}^\pm[k, \Delta\ell]$ -shrinking points and stability loss boundaries are independent of k . We denote the leading order components by $\theta_{\Delta\ell}^\pm$ and provide formulas for them in Appendix B.

2.4 Nearly-hyperbolic annular sectors

Let $\Delta\ell \in \mathbb{Z}$ and a choice of $+$ or $-$ be given. Suppose $\kappa_{\Delta\ell}^\pm$ and $\kappa_{\Delta\ell-1}^\pm$ are non-zero (as is generically the case) with which $\theta_{\Delta\ell}^\pm$ and $\theta_{\Delta\ell-1}^\pm$ are well-defined. Assuming admissibility, for any sufficiently large value of $k \in \mathbb{Z}$ the inner boundary of the \mathcal{G}_k^\pm -mode-locking region, call it γ_k , is C^K between endpoints, call them p_k and q_k , at $\theta = \theta_{\Delta\ell}^\pm + \mathcal{O}(\frac{1}{k})$ and $\theta = \theta_{\Delta\ell-1}^\pm + \mathcal{O}(\frac{1}{k})$. If $\kappa_{\Delta\ell}^\pm > 0$, then p_k is a $\mathcal{G}^\pm[k, \Delta\ell]$ -shrinking point, while if $\kappa_{\Delta\ell}^\pm < 0$, then at p_k there is an $\mathcal{G}^\pm[k, \Delta\ell]$ -cycle with a stability multiplier of -1 . Similarly if $\kappa_{\Delta\ell-1}^\pm > 0$, then q_k is a $\mathcal{G}^\pm[k, \Delta\ell - 1]$ -shrinking point, while if $\kappa_{\Delta\ell-1}^\pm < 0$, then at q_k there is an $\mathcal{G}^\pm[k, \Delta\ell - 1]$ -cycle with a stability multiplier of -1 .

We define $\Sigma_{k, \Delta\ell}^\pm$ as the region bounded by the curves γ_k and γ_{k+1} , the line segment connecting p_k and p_{k+1} , and the line segment connecting q_k and q_{k+1} . The boundaries γ_k and γ_{k+1} are given by (2.20), which resembles a hyperbola, while θ is approximately constant along the two line segments. In this sense $\Sigma_{k, \Delta\ell}^\pm$ is a “nearly-hyperbolic annular sector”.

Equations (2.20) and (B.3)–(B.4) provide expressions for the boundaries of $\Sigma_{k, \Delta\ell}^\pm$ with an $\mathcal{O}(\frac{1}{k^2})$ error. Fig. 4 illustrates the leading order approximation for the example of Fig. 3.

For a given value of $\Delta\ell$ and a choice of $+$ or $-$, let $r_k(\theta)$ denote the radial coordinate of γ_k (i.e. the inner boundary of the \mathcal{G}_k^\pm -mode-locking region) for each k . Extending (2.20), we have $r_k(\theta) = \frac{1}{k}\Gamma(\theta) + \frac{1}{k^2}\Gamma_2(\theta) + \mathcal{O}(\frac{1}{k^3})$, for a C^K function Γ_2 . The difference in r -values between the inner and outer boundaries of $\Sigma_{k, \Delta\ell}^\pm$ is then

$$r_k(\theta) - r_{k+1}(\theta) = \frac{1}{k^2}\Gamma(\theta) + \mathcal{O}\left(\frac{1}{k^3}\right), \quad (2.22)$$

because $\mathcal{O}(\frac{1}{k^2})$ -terms involving Γ_2 vanish.

We then define

$$\delta := \frac{1}{k} \left(1 - \frac{r}{r_k(\theta)} \right), \quad (2.23)$$

with which each point in $\Sigma_{k, \Delta\ell}^\pm$ is uniquely represented by the pair (δ, θ) . We have $\delta = 0$ at any point on the outer boundary of $\Sigma_{k, \Delta\ell}^\pm$ and by (2.22) we have $\delta = \frac{1}{k^2} + \mathcal{O}(\frac{1}{k^3})$ at any point on the inner boundary of $\Sigma_{k, \Delta\ell}^\pm$. Let

$$\theta_{\min} := \min(\theta_{\Delta\ell}^\pm, \theta_{\Delta\ell-1}^\pm), \quad \theta_{\max} := \max(\theta_{\Delta\ell}^\pm, \theta_{\Delta\ell-1}^\pm). \quad (2.24)$$

On the two linear boundaries of $\Sigma_{k,\Delta\ell}^\pm$, we have $\theta = \theta_{\min} + \mathcal{O}(\frac{1}{k})$ and $\theta = \theta_{\max} + \mathcal{O}(\frac{1}{k})$.

The particular definition (2.23) is useful because, to leading order, $\Sigma_{k,\Delta\ell}^\pm$ is a rectangle in (δ, θ) -coordinates as given by (1.8). We include the factor $\frac{1}{k}$ in (2.23) so that an $\mathcal{O}(1)$ change in the value of δ corresponds to an $\mathcal{O}(1)$ change in the value of r .

2.5 The approximation by skew sawtooth maps

Throughout each sector $\Sigma_{k,\Delta\ell}^\pm$ we can approximate the dynamics of (1.2) by using the skew sawtooth map (1.5) with appropriate formulas for a_L , a_R and w in terms of δ and θ . The value of w is independent of θ and given by

$$w = k^2 \delta. \quad (2.25)$$

The values of a_L and a_R are independent of δ and given in Table 1. Note that we do not consider sectors with $\kappa_{\Delta\ell}^\pm < 0$ and $\kappa_{\Delta\ell-1}^\pm < 0$ as such sectors do not seem to involve admissible $\mathcal{G}^\pm[k, \Delta\ell]$ -cycles.

As indicated in Table 1, the formulas for a_L and a_R take slightly different forms in different cases, but in each case $\frac{a_R}{a_L}$ is constant throughout $\Sigma_{k,\Delta\ell}^\pm$. Therefore the value of $\frac{a_R}{a_L}$ characterises the two-dimensional slice of parameter space of (1.5) to which $\Sigma_{k,\Delta\ell}^\pm$ corresponds. In terms of a_L , a_R , and w , in the approximation of (1.8) the four parts of the boundary of $\Sigma_{k,\Delta\ell}^\pm$ are given by $w = 0$, $w = 1$, $a_R = 1$, and either $a_L = 1$ or $a_L = -1$.

One iteration of the skew sawtooth map (1.5) corresponds to many iterations of (1.2). To be more specific, let

$$g_{\text{lift}}(z) := \begin{cases} w + a_L(z_i - z_{\text{sw}}) + z_{\text{sw}}, & 0 \leq z_i \leq z_{\text{sw}}, \\ w + a_R(z_i - z_{\text{sw}}) + z_{\text{sw}}, & z_{\text{sw}} \leq z_i < 1, \end{cases} \quad (2.26)$$

be a lift of g . At any point in $\Sigma_{k,\Delta\ell}^\pm$, for all but an $\mathcal{O}(\frac{1}{k})$ set of z -values for which (1.2) and (1.5) are misaligned, if $0 \leq z \leq z_{\text{sw}}$ then $g(z)$ corresponds to $f^{\mathcal{G}^\pm[k+\Delta k, \Delta\ell]}$, while if $z_{\text{sw}} \leq z < 1$ then $g(z)$ corresponds to $f^{\mathcal{G}^\pm[k+\Delta k, \Delta\ell-1]}$, where

$$\Delta k = g_{\text{lift}}(z) - g(z). \quad (2.27)$$

A formal statement of this approximation is given below by Theorem 5.2.

	a_L	a_R
for $\Sigma_{k,\Delta\ell}^+$ with $\kappa_{\Delta\ell}^+ > 0$, $\kappa_{\Delta\ell-1}^+ > 0$	$\frac{\tan(\theta)}{\tan(\theta_{\min})}$	$\frac{\tan(\theta)}{\tan(\theta_{\max})}$
for $\Sigma_{k,\Delta\ell}^+$ with $\kappa_{\Delta\ell}^+ \kappa_{\Delta\ell-1}^+ < 0$	$-\frac{\tan(\theta)}{\tan(\theta_{\min})}$	$\frac{\tan(\theta)}{\tan(\theta_{\max})}$
for $\Sigma_{k,\Delta\ell}^-$ with $\kappa_{\Delta\ell}^- > 0$, $\kappa_{\Delta\ell-1}^- > 0$	$\frac{\tan(\theta_{\max})}{\tan(\theta)}$	$\frac{\tan(\theta_{\min})}{\tan(\theta)}$
for $\Sigma_{k,\Delta\ell}^-$ with $\kappa_{\Delta\ell}^- \kappa_{\Delta\ell-1}^- < 0$	$-\frac{\tan(\theta_{\max})}{\tan(\theta)}$	$\frac{\tan(\theta_{\min})}{\tan(\theta)}$

Table 1: Formulas for a_L and a_R inside a sector $\Sigma_{k,\Delta\ell}^\pm$.

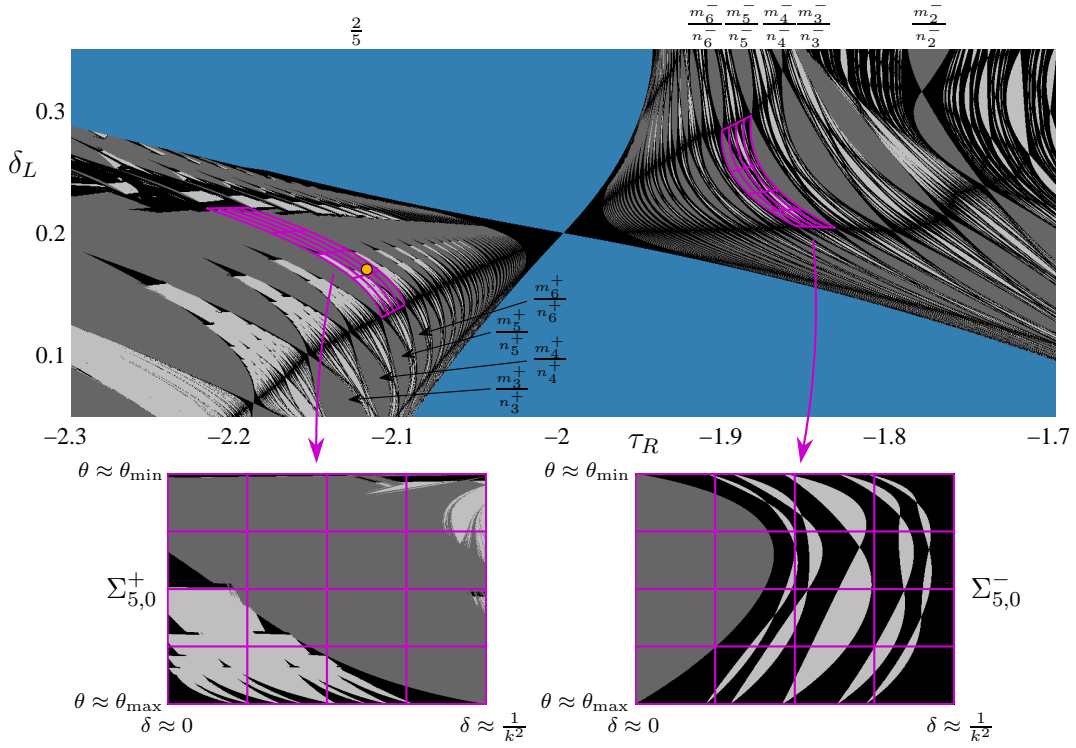


Figure 7: A magnification of Fig. 1 centred about the \mathcal{S} -shrinking point with $\mathcal{S} = \mathcal{F}[2, 2, 5] = LRRLR$ computed in the same way as Fig. 3. Here $\frac{m}{n} = \frac{2}{5}$ and the Farey roots are $\frac{m^-}{n^-} = \frac{1}{3}$ and $\frac{m^+}{n^+} = \frac{1}{2}$. For $\Sigma_{5,0}^+$, $\theta_{\min} = \theta_0^+ \approx 4.9786$ and $\theta_{\max} = \theta_{-1}^+ \approx 6.0014$. For $\Sigma_{5,0}^-$, $\theta_{\min} = \theta_0^- \approx 2.2254$ and $\theta_{\max} = \theta_{-1}^- \approx 3.0811$. The dot inside $\Sigma_{5,0}^+$ indicates the parameter values of Fig. 11-B.

2.6 Dynamics of skew sawtooth maps

If $\frac{a_R}{a_L} > 0$, as in both plots shown in Fig. 5, then (1.5) is a homeomorphism and has a unique rotation number. The dynamics of (1.5) approximates that of (1.2), not only in $\Sigma_{2,0}^+$ and $\Sigma_{3,1}^+$, but also in $\Sigma_{k,0}^+$ and $\Sigma_{k,1}^+$ for all $k \geq 1$, see Fig. 3.

For instance in the large grey region of the left plot of Fig. 5, the map (1.5) has a stable fixed point with $0 \leq z \leq z_{\text{sw}}$ and $g_{\text{lift}}(z) - g(z) = 1$. Therefore, in the corresponding region of each $\Sigma_{k,0}^+$, the map (1.2) has a stable $\mathcal{G}^+[k+1, 0]$ -cycle (this belongs to the \mathcal{G}_{k+1}^+ -mode-locking-region).

As a further illustration, consider the mode-locking region of the left plot of Fig. 5 with rotation number $\frac{1}{2}$. This region has two components connected by a shrinking point. The map (1.5) has a stable period-two solution $\{z_0, z_1\}$ with $g_{\text{lift}}(z_0) - g(z_0) = 0$, $g_{\text{lift}}(z_1) - g(z_1) = 1$, $0 \leq z_0 \leq z_{\text{sw}}$, and $0 \leq z_1 \leq z_{\text{sw}}$ in the upper component, and a stable period-two solution $\{z_0, z_1\}$ with the same properties except $z_{\text{sw}} \leq z_1 < 1$ in the lower component. Therefore, in the upper [resp. lower] component of each $\Sigma_{k,0}^+$, the map (1.2) has a stable $\mathcal{G}^+[k, 0]\mathcal{G}^+[k+1, 0]$ -cycle [resp. $\mathcal{G}^+[k, 0]\mathcal{G}^+[k+1, -1]$ -cycle]. These belong to a mode-locking region with rotation number $\frac{m_k^+ + m_{k+1}^+}{n_k^+ + n_{k+1}^+}$. In this way (1.5) can be used to describe all mode-locking regions of (1.2) near a shrinking point.

Fig. 7 shows a second example using the \mathcal{S} -shrinking point of Fig. 1 with $\mathcal{S} = LRRLR$.

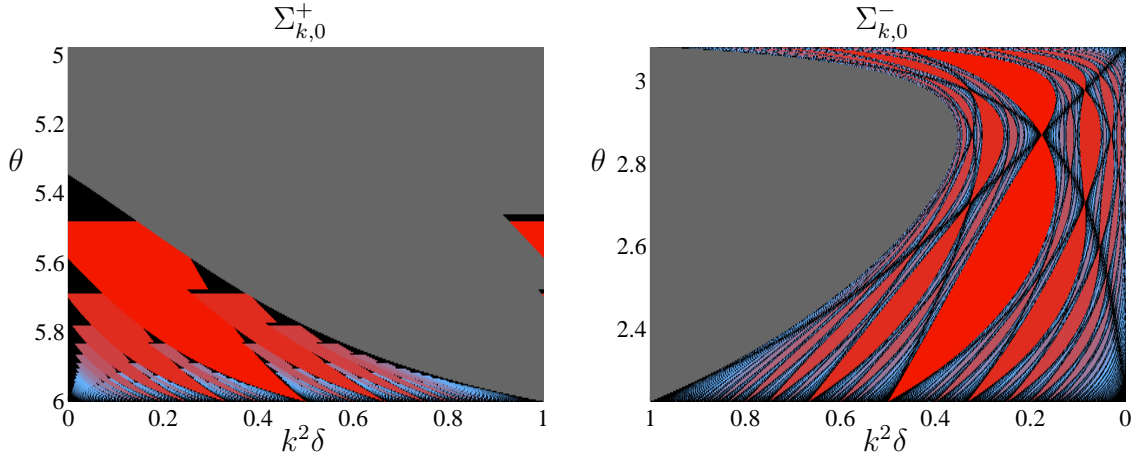


Figure 8: Mode-locking regions of (1.5) with (1.9) corresponding to $\Sigma_{k,0}^+$ and $\Sigma_{k,0}^-$ of Fig. 7, where $k \in \mathbb{Z}^+$. For $\Sigma_{k,0}^+$, $\frac{a_R}{a_L} = -12\frac{2}{3}$. For $\Sigma_{k,0}^-$, $\frac{a_R}{a_L} = 21\frac{1}{2}$. In both plots the axes are oriented to match Fig. 7.

The sectors $\Sigma_{5,0}^+$ and $\Sigma_{5,0}^-$ are highlighted and Fig. 8 shows the mode-locking regions of (1.5) corresponding to these sectors.

As expected, the dynamics of (1.5) shown in Fig. 8 matches well to the dynamics of (1.2) in $\Sigma_{5,0}^+$ and $\Sigma_{5,0}^-$ shown in Fig. 7. For each $\Sigma_{k,0}^-$, we have $\frac{a_R}{a_L} = 21\frac{1}{2}$, and so the right plot of Fig. 8 is similar to the left plot of Fig. 5 (for which $\frac{a_R}{a_L} \approx 14.7884$). For each $\Sigma_{k,0}^+$, we have $\frac{a_R}{a_L} = -12\frac{2}{3}$. Here $\frac{a_R}{a_L} < 0$ because $\kappa_0^+ < 0$ (thus $\mathcal{G}^+[k, 0]$ -shrinking points do not exist) and $\kappa_{-1}^+ > 0$, see Table 1. With $\frac{a_R}{a_L} < 0$, the map (1.5) is not invertible and exhibits a fundamentally different bifurcation structure. There are no shrinking points. Mode-locking regions emanate from $\theta = \theta_{\max}$ and terminate at critical values of θ where the corresponding periodic solution attains a stability multiplier of -1 . Beyond these critical values the dynamics of (1.5) can be chaotic and multiple attractors exist for some parameter values [17].

3 A centre manifold and approximately recurrent dynamics

In this section we first discuss symmetries of the centre manifolds associated with an \mathcal{S} -shrinking point to explain why the majority of the calculations involve the map $f^{\mathcal{S}(-d)}$, §3.1. We then derive new properties of $\mathcal{G}^+[k, \Delta\ell]$ in the case $\Delta\ell \geq 0$, §3.2. In §3.3 we describe the dynamics of $f^{\mathcal{S}(-d)}$ in relation to its centre manifold and in §3.4 identify a fundamental domain of this manifold.

3.1 Centre manifolds

At an \mathcal{S} -shrinking point (1.2) has a unique \mathcal{S}^0 -cycle, denoted $\{y_i\}$. There are also uncountably many \mathcal{S} -cycles and the union of these forms a non-planar polygon with vertices y_i , see Fig. 9.

Each point on the line passing through y_0 and y_d is a fixed point of $f^{\mathcal{S}}$. Of these, only points between y_0 and y_d are admissible (i.e. are fixed points of f^n). More generally, for each

$j = 0, 1, \dots, n-1$, every point on the line passing through y_j and $y_{(d+j) \bmod n}$ is a fixed point of $f^{\mathcal{S}^{(j)}}$. Each line is a centre manifold persisting as an extended centre manifold for parameter values near the \mathcal{S} -shrinking point.

As shown in [1], the dynamics near an \mathcal{S} -shrinking point can be analysed by working with these (extended) centre manifolds for the four values $j \in \{0, (\ell-1)d, \ell d, -d\}$, where from now on we omit “mod n ” in indices for brevity. These four values of j correspond to the four line segments of the polygon that intersect the switching manifold. Also, the four curves that bound the mode-locking region associated with the \mathcal{S} -shrinking point are where the j^{th} point of an \mathcal{S} -cycle lies on the switching manifold for these four values of j .

For the remainder of this paper we work only with the $j = -d$ centre manifold. As explained in the next section, we can use this manifold to extract information about $\mathcal{G}^+[k, \Delta\ell]$ -cycles with $\Delta\ell \geq 0$. Information about $\mathcal{G}^+[k, \Delta\ell]$ -cycles with $\Delta\ell < 0$ and $\mathcal{G}^-[k, \Delta\ell]$ -cycles can be deduced by utilising two forms of symmetry associated with shrinking points. First, we can simply swap the symbols L and R throughout the analysis. More accurately, if we flip all the symbols of $\mathcal{F}[\ell, m, n]$ (from L to R and vice-versa) we produce $\mathcal{F}[n-\ell, m, n]^{(\ell d)}$. Second, rather than viewing $\mathcal{F}[\ell, m, n]$ as clockwise rotation with rotation number $\frac{m}{n}$, we can view it as anticlockwise rotation with rotation number $\frac{n-m}{n}$. This corresponds to the identity $\mathcal{F}[\ell, n-m, n] = \mathcal{F}[\ell, m, n]^{((\ell-1)d)}$. It follows that by replacing ℓ and m with $n-\ell$ and $n-m$, respectively, in the results below we can generate analogous results for any $\mathcal{G}^\pm[k, \Delta\ell]$ -cycle.

3.2 Properties of $\mathcal{G}^+[k, \Delta\ell]$ with $\Delta\ell \geq 0$

Here we provide three symbolic results for $\mathcal{G}^+[k, \Delta\ell]$ with $\Delta\ell \geq 0$ obtained in a straight-forward manner from formulas given in [1]. Here it is helpful to work with words rather than sequences. As explained in [1], any periodic symbol sequence \mathcal{S} of minimal period n is given by the infinite repetition of the primitive word $\mathcal{S}_0 \cdots \mathcal{S}_{n-1}$. In this way there is a one-to-one correspondence between periodic symbol sequences and primitive words, and so we also denote the word $\mathcal{S}_0 \cdots \mathcal{S}_{n-1}$ by \mathcal{S} .

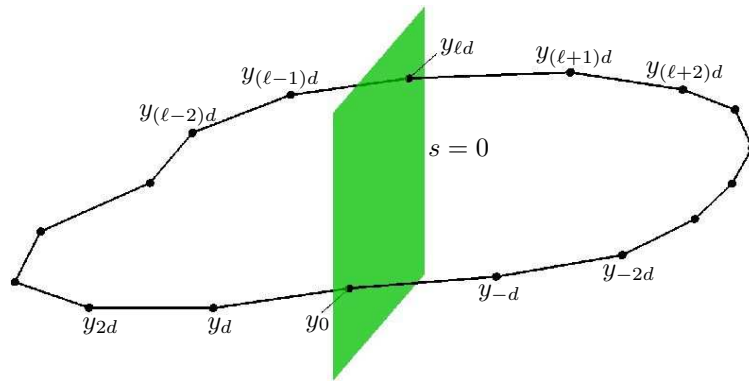


Figure 9: A sketch of the uncountable collection of \mathcal{S} -cycles of (1.2) at an \mathcal{S} -shrinking point.

For any $\mathcal{S} = \mathcal{F}[\ell, m, n]$, we define the words

$$\mathcal{X} := \mathcal{S}_0 \cdots \mathcal{S}_{(\ell d - 1) \bmod n} , \quad (3.1)$$

$$\mathcal{Y} := \mathcal{S}_{\ell d \bmod n} \cdots \mathcal{S}_{n-1} , \quad (3.2)$$

$$\hat{\mathcal{X}} := \mathcal{S}_0 \cdots \mathcal{S}_{(-d-1) \bmod n} . \quad (3.3)$$

We first show that the word $\mathcal{G}^+[k, \Delta\ell]$ ends in powers of $\mathcal{S}^{(-d)}$.

Lemma 3.1. *For all $k \in \mathbb{Z}^+$ and $\Delta\ell = 0, \dots, k-1$,*

$$\mathcal{G}^+[k, \Delta\ell] = \left(\mathcal{X} \mathcal{Y}^{\bar{0}} \right)^{\Delta\ell} \hat{\mathcal{X}} (\mathcal{S}^{(-d)})^{k-\Delta\ell} . \quad (3.4)$$

Proof. By Proposition 4.8 of [1], $\mathcal{G}^+[k, \Delta\ell] = \left(\mathcal{X} \mathcal{Y}^{\bar{0}} \right)^{\Delta\ell} \mathcal{S}^{k-\Delta\ell} \hat{\mathcal{X}}$. This can be rewritten as (3.4) because $\mathcal{S} \hat{\mathcal{X}} = \hat{\mathcal{X}} \mathcal{S}^{(-d)}$. \square

The next result shows that if we flip the first symbol of $\mathcal{G}^+[k, \Delta\ell]$ the result is a cyclic permutation of $\mathcal{G}^+[k, \Delta\ell - 1]$.

Lemma 3.2. *For all $k \in \mathbb{Z}^+$ and $\Delta\ell = 0, \dots, k-1$,*

$$\mathcal{G}^+[k, \Delta\ell]^{\bar{0}} = \mathcal{G}^+[k, \Delta\ell - 1]^{(-d_k^+)} . \quad (3.5)$$

Proof. The result is obtained by simply applying the general identity $\mathcal{F}[\ell, m, n]^{\bar{0}} = \mathcal{F}[\ell - 1, m, n]^{(-d)}$ (equation (4.3) of [1]) to $\mathcal{G}^+[k, \Delta\ell] = \mathcal{F}[\ell_k^+ + \Delta\ell, m_k^+, n_k^+]$. \square

The $j = -d$ centre manifold is useful for analysing $\mathcal{G}^+[k, \Delta\ell]$ -cycles with $\Delta\ell \geq 0$ because, by Lemma 3.1, the word $\mathcal{G}^+[k, \Delta\ell]$ ends in a large power of $\mathcal{S}^{(-d)}$. Thus, under certain assumptions, the fixed point of $f^{\mathcal{G}^+[k, \Delta\ell]}$ lies close to the $j = -d$ centre manifold. Also, by Lemma 3.2, $\mathcal{G}^+[k, \Delta\ell - 1]$ -cycles can be analysed by studying the fixed point of $f^{\mathcal{G}^+[k, \Delta\ell]^{\bar{0}}}$ which lies close to the $j = -d$ centre manifold for the same reason.

We also provide an additional result used in later proofs.

Lemma 3.3. *For all $k \in \mathbb{Z}^+$ and $\Delta\ell = 0, \dots, k-1$,*

$$\mathcal{S}^{(-d)} \mathcal{G}^+[k, \Delta\ell] = \mathcal{G}^+[k, \Delta\ell]^{\bar{0} \overline{(\ell_k^+ + \Delta\ell) d_k^+}} \mathcal{S}^{(-d)} . \quad (3.6)$$

Proof. Since $d_k^+ = n$ (see Lemma 4.5 of [1]), by (3.4),

$$\mathcal{G}^+[k, \Delta\ell]^{(-d_k^+)} = \mathcal{S}^{(-d)} \left(\mathcal{X} \mathcal{Y}^{\bar{0}} \right)^{\Delta\ell} \hat{\mathcal{X}} (\mathcal{S}^{(-d)})^{k-\Delta\ell-1} . \quad (3.7)$$

Also, by (2.9),

$$\mathcal{G}^+[k, \Delta\ell]^{\bar{0} \overline{(\ell_k^+ + \Delta\ell) d_k^+}} = \mathcal{G}^+[k, \Delta\ell]^{(-d_k^+)} . \quad (3.8)$$

Then (3.6) is obtained by combining (3.4), (3.7) and (3.8). \square

3.3 Dynamics near the centre manifold

The map $f^{\mathcal{S}^{(-d)}}$ is affine with matrix part $M_{\mathcal{S}^{(-d)}}$. At the \mathcal{S} -shrinking point, $(\eta, \nu) = (0, 0)$, $M_{\mathcal{S}^{(-d)}}$ has a unit eigenvalue with multiplicity one. Thus in a neighbourhood of $(\eta, \nu) = (0, 0)$, $M_{\mathcal{S}^{(-d)}}$ has an eigenvalue $\lambda(\eta, \nu)$ with $\lambda(0, 0) = 1$ and a C^K dependency on η and ν . Throughout this neighbourhood let ω_{-d}^\top and ζ_{-d} be the corresponding left and right eigenvectors of $M_{\mathcal{S}^{(-d)}}$ normalised by

$$e_1^\top \zeta_{-d} = 1, \quad \omega_{-d}^\top \zeta_{-d} = 1. \quad (3.9)$$

At points (η, ν) where $\lambda \neq 1$, the \mathcal{S} -cycle, denoted $\{x_i^{\mathcal{S}}\}$, is unique. The point $x_{-d}^{\mathcal{S}}$ is a fixed point of $f^{\mathcal{S}^{(-d)}}$. As shown in [1] (Lemma 7.2), the quantities

$$x_{-d}^{\text{int}} := (I - \zeta_{-d} e_1^\top) x_{-d}^{\mathcal{S}}, \quad s_{-d}^{\text{step}} := (1 - \lambda) e_1^\top x_{-d}^{\mathcal{S}}, \quad (3.10)$$

whose purpose is explained below, can be extended in a C^K fashion to a neighbourhood of $(\eta, \nu) = (0, 0)$ (i.e. including points where $\lambda = 1$).

We define two functions $u : \mathbb{R}^N \rightarrow \mathbb{R}$ and $v : \mathbb{R} \rightarrow \mathbb{R}^N$ by

$$u(x) := \omega_{-d}^\top (x - x_{-d}^{\text{int}}), \quad v(h) := x_{-d}^{\text{int}} + h \zeta_{-d}. \quad (3.11)$$

The line

$$W^c := \{v(h) \mid h \in \mathbb{R}\}, \quad (3.12)$$

has direction ζ_{-d} and passes through $x_{-d}^{\mathcal{S}}$ whenever $\lambda \neq 1$ and so is a centre manifold of $f^{\mathcal{S}^{(-d)}}$.

Any $x \in \mathbb{R}^N$ can be uniquely written as

$$x = x_{-d}^{\text{int}} + h \zeta_{-d} + q, \quad (3.13)$$

where $h \in \mathbb{R}$ and $q \in \mathbb{R}^N$ satisfies $\omega_{-d}^\top q = 0$ (equation (3.13) represents a partial decomposition by eigenspaces). Moreover, h and q are given by

$$h = u(x), \quad q = (I - \zeta_{-d} \omega_{-d}^\top) (x - x_{-d}^{\text{int}}), \quad (3.14)$$

and $x \in W^c$ if and only if $q = 0$.

In terms of the decomposition (3.13), we can write an arbitrary power of $f^{\mathcal{S}^{(-d)}}$ as

$$f^{(\mathcal{S}^{(-d)})^k}(x) = x_{-d}^{\text{int}} + \left(s_{-d}^{\text{step}} \sum_{j=0}^{k-1} \lambda^j + h \lambda^k \right) \zeta_{-d} + M_{\mathcal{S}^{(-d)}}^k q, \quad (3.15)$$

valid for any $x \in \mathbb{R}^N$ and any $k \in \mathbb{Z}^+$. This is illustrated in Fig. 10. Equation (3.15) has the form (3.13) because the middle term is a scalar multiple of ζ_j and the last term is orthogonal to ω_j .

In summary, the function u returns the value of h in the decomposition (3.13), while the function v defines the centre manifold W^c . The composition $v \circ u$ represents the projection onto W^c in directions orthogonal to ω_{-d} . The point x_{-d}^{int} is the intersection of W^c with the switching manifold, while $s_{-d}^{\text{step}} = u\left(f^{\mathcal{S}^{(-d)}}(x_{-d}^{\text{int}})\right)$ is a scalar quantity used in (3.15) to describe the action of iteration under $f^{\mathcal{S}^{(-d)}}$.

If $\rho_{\max} < 1$, where ρ_{\max} is defined by (2.14), then forward orbits of $f^{S(-d)}$ approach W^c . Indeed, by (3.15) the vector $M_{S(-d)}^k q$ is the displacement of $\left(f^{S(-d)}\right)^k(x)$ from W^c in directions orthogonal to ω_{-d} . If $\rho_{\max} < 1$, then $M_{S(-d)}^k q = \mathcal{O}(\rho_{\max}^k)$ for any fixed q orthogonal to ω_{-d} . In view of (3.14) we can therefore write

$$M_{S(-d)}^k (I - \zeta_{-d} \omega_{-d}^T) = \mathcal{O}(\rho_{\max}^k). \quad (3.16)$$

3.4 An approximately recurrent line segment, $\Omega_{\Delta\ell}$

Here we identify a useful fundamental domain $\Omega_{\Delta\ell} \subset W^c$, then provide three lemmas. Lemma 3.4 gives an algebraic identity, Lemma 3.5 indicates the rough range of η and ν values relevant for $\Omega_{\Delta\ell}$, and Lemma 3.6 relates $\Omega_{\Delta\ell}$ to a boundary of the \mathcal{G}_k^+ -mode-locking region.

For any $\tilde{x} \in W^c$, consider a half-open line segment with endpoints \tilde{x} and $f^{S(-d)}(\tilde{x})$. Assuming $\tilde{x} \neq x_{-d}^S$ (in the generic case $\lambda \neq 1$ that x_{-d}^S exists), all orbits of $f^{S(-d)}$ in W^c on one side of x_{-d}^S have exactly one point in this line segment, and in this sense the line segment is a fundamental domain.

We choose $\tilde{x} \in W^c$ such that its image under $f^{\mathcal{X}\bar{0}(\mathcal{Y}\bar{0}\mathcal{X})^{\Delta\ell}}$ lies on the switching manifold. We do this because by (3.4) the first $(\ell_k^+ + \Delta\ell) d_k^+$ symbols of $\mathcal{G}^+[k, \Delta\ell]$ are $(\mathcal{X}\mathcal{Y}\bar{0})^{\Delta\ell} \hat{\mathcal{X}}$, which, upon flipping the first symbol, can be rewritten as $\mathcal{X}\bar{0}(\mathcal{Y}\bar{0}\mathcal{X})^{\Delta\ell}$. Thus if there exists a $\mathcal{G}^+[k, \Delta\ell]^{\bar{0}}$ -cycle for which $f^{\mathcal{X}\bar{0}(\mathcal{Y}\bar{0}\mathcal{X})^{\Delta\ell}}(x_0^{\mathcal{G}^+[k, \Delta\ell]^{\bar{0}}})$ lies on the switching manifold, then the $\mathcal{G}^+[k, \Delta\ell]^{\bar{0}}$ -cycle is also a $\mathcal{G}^+[k, \Delta\ell]^{\bar{0}}(\ell_k^+ + \Delta\ell) d_k^+$ -cycle, and by (2.9) it is also a permutation of a $\mathcal{G}^+[k, \Delta\ell]$ -cycle.

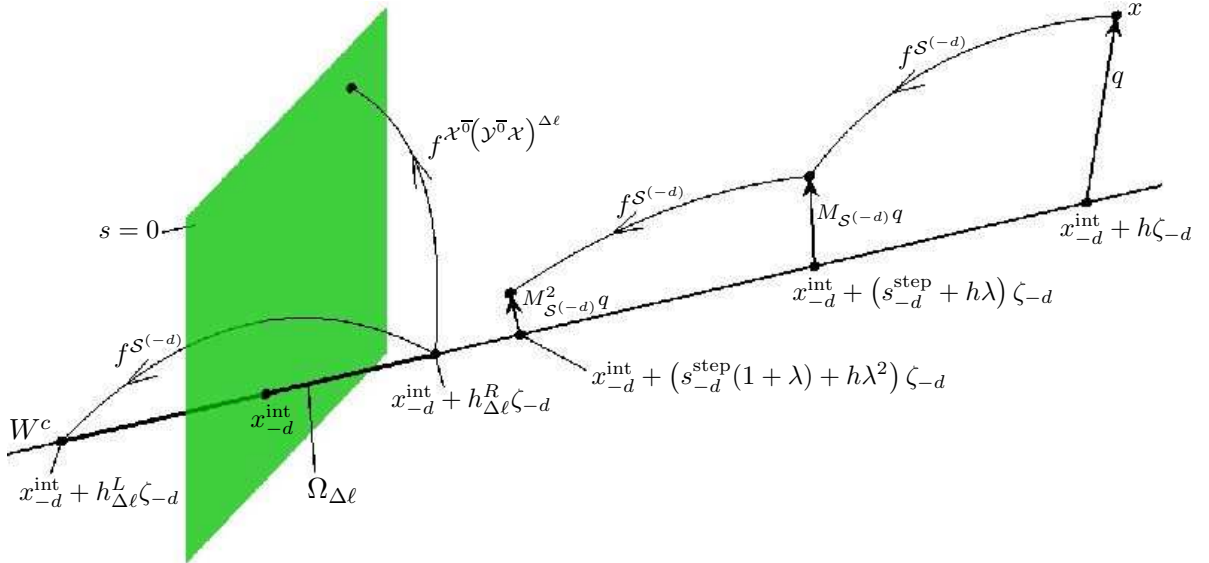


Figure 10: A sketch illustrating dynamics near the centre manifold W^c (3.12). We show an arbitrary point x and its first and second images under $f^{S(-d)}$ and indicate the decomposition of these points as given by (3.15). We also show the fundamental domain $\Omega_{\Delta\ell}$ (3.19).

That is, we let $\tilde{x} = v(h_{\Delta\ell}^R)$, where $h_{\Delta\ell}^R \in \mathbb{R}$ is defined by

$$e_1^\top f^{\mathcal{X}\bar{\mathcal{O}}(\mathcal{Y}\bar{\mathcal{O}}\mathcal{X})^{\Delta\ell}}(v(h_{\Delta\ell}^R)) = 0. \quad (3.17)$$

The image of $v(h_{\Delta\ell}^R)$ under $f^{\mathcal{S}^{(-d)}}$ is $v(h_{\Delta\ell}^L)$ where

$$h_{\Delta\ell}^L := e_1^\top f^{\mathcal{S}^{(-d)}}(v(h_{\Delta\ell}^R)). \quad (3.18)$$

Then our fundamental domain is

$$\Omega_{\Delta\ell} := \left\{ v(h) \mid h_{\Delta\ell}^L \leq h < h_{\Delta\ell}^R \right\}, \quad (3.19)$$

assuming $h_{\Delta\ell}^L < h_{\Delta\ell}^R$.

Before we continue we must verify that $h_{\Delta\ell}^R$ is unique and well-defined by (3.17). To do this we solve for $h_{\Delta\ell}^R$ in (3.17) giving

$$h_{\Delta\ell}^R = - \frac{e_1^\top f^{\mathcal{X}\bar{\mathcal{O}}(\mathcal{Y}\bar{\mathcal{O}}\mathcal{X})^{\Delta\ell}}(x_{-d}^{\text{int}})}{e_1^\top M_{\mathcal{X}\bar{\mathcal{O}}(\mathcal{Y}\bar{\mathcal{O}}\mathcal{X})^{\Delta\ell}\zeta_{-d}}}, \quad (3.20)$$

assuming that the denominator of (3.20) is non-zero. Next we derive an explicit expression for the leading order component of this denominator. Then Lemma 3.5 gives formulas for $h_{\Delta\ell}^L$ and $h_{\Delta\ell}^R$ and is proved in Appendix A.

Lemma 3.4.

Suppose $\det(J) \neq 0$. Then for any $\Delta\ell \geq 0$,

$$e_1^\top M_{\mathcal{X}\bar{\mathcal{O}}(\mathcal{Y}\bar{\mathcal{O}}\mathcal{X})^{\Delta\ell}\zeta_{-d}} = \begin{cases} \frac{t_{(\ell-1)d}}{t_{-d}} + \mathcal{O}(\eta, \nu), & \Delta\ell = 0, \\ \frac{ct_{(\ell-1)d}}{at_{-d}} (\kappa_{\Delta\ell}^+ - \kappa_{\Delta\ell-1}^+) + \mathcal{O}(\eta, \nu), & \Delta\ell \geq 1. \end{cases} \quad (3.21)$$

Proof. If $\Delta\ell = 0$, then the denominator of (3.20) is $e_1^\top M_{\mathcal{X}\bar{\mathcal{O}}\zeta_{-d}}$ and the result follows immediately from equation (6.9) of [1]. If $\Delta\ell \geq 1$, then at $(\eta, \nu) = (0, 0)$ we have

$$u_0^\top (I - M_{\mathcal{S}^{\bar{t}d}}) = \frac{bt_d}{ct_{(\ell+1)d}} e_1^\top M_{\mathcal{X}}, \quad (3.22)$$

where u_0^\top is the left eigenvector of $M_{\mathcal{S}}$ corresponding to the unit eigenvalue 1 (this is equation (A.34) of [1]). Also

$$\mathcal{X}\bar{\mathcal{O}}(\mathcal{Y}\bar{\mathcal{O}}\mathcal{X})^{\Delta\ell} = \mathcal{X}\bar{\mathcal{O}}\mathcal{Y}\bar{\mathcal{O}}(\mathcal{X}\mathcal{Y}\bar{\mathcal{O}})^{\Delta\ell-1}\mathcal{X} = \mathcal{S}^{(-d)}(\mathcal{S}^{\bar{t}d})^{\Delta\ell-1}\mathcal{X},$$

and so by (3.22) at $(\eta, \nu) = (0, 0)$ we have

$$e_1^\top M_{\mathcal{X}\bar{\mathcal{O}}(\mathcal{Y}\bar{\mathcal{O}}\mathcal{X})^{\Delta\ell}\zeta_{-d}} = \frac{ct_{(\ell+1)d}}{bt_d} u_0^\top (I - M_{\mathcal{S}^{\bar{t}d}}) M_{\mathcal{S}^{\bar{t}d}}^{\Delta\ell-1} \zeta_{-d}.$$

This yields (3.21) for $\Delta\ell \geq 1$ by using (2.13) and the definition of $\kappa_{\Delta\ell}^+$ (B.1). \square

Lemma 3.5.

Suppose $\det(J) \neq 0$. Then for any $\Delta\ell \geq 0$,

$$h_{\Delta\ell}^L = \begin{cases} \eta - \frac{t_d \kappa_{-1}^+}{t_{(\ell+1)d}} \nu + \mathcal{O}((\eta, \nu)^2), & \Delta\ell = 0, \\ \frac{a}{c(\kappa_{\Delta\ell}^+ - \kappa_{\Delta\ell-1}^+)} \left(\eta - \frac{t_{-d} \kappa_{\Delta\ell-1}^+}{t_{(\ell-1)d}} \nu \right) + \mathcal{O}((\eta, \nu)^2), & \Delta\ell \geq 1, \end{cases} \quad (3.23)$$

$$h_{\Delta\ell}^R = \begin{cases} \eta - \frac{t_{-d} \kappa_0^+}{t_{(\ell-1)d}} \nu + \mathcal{O}((\eta, \nu)^2), & \Delta\ell = 0, \\ \frac{a}{c(\kappa_{\Delta\ell}^+ - \kappa_{\Delta\ell-1}^+)} \left(\eta - \frac{t_{-d} \kappa_{\Delta\ell}^+}{t_{(\ell-1)d}} \nu \right) + \mathcal{O}((\eta, \nu)^2), & \Delta\ell \geq 1, \end{cases} \quad (3.24)$$

assuming $\kappa_{\Delta\ell}^+ \neq \kappa_{\Delta\ell-1}^+$ in the case $\Delta\ell \geq 1$.

Inside the \mathcal{G}_k^+ -mode-locking region and between the $\mathcal{G}^+[k, \Delta\ell]$ and $\mathcal{G}^+[k, \Delta\ell - 1]$ -shrinking points (if they exist), there are $\mathcal{G}^+[k, \Delta\ell]$ and $\mathcal{G}^+[k, \Delta\ell - 1]$ -cycles, one of which is attracting (as determined by the sign of a). The mode-locking region is bounded by a curve where $x_0^{\mathcal{G}^+[k, \Delta\ell]}$ lies on the switching manifold, and a curve where $x_{(\ell_k^+ + \Delta\ell - 1)d_k^+}^{\mathcal{G}^+[k, \Delta\ell]}$ lies on the switching manifold. These boundaries are where $P_{\mathcal{G}^+[k, \Delta\ell](i)}$ is singular for $i = 0$ and $i = (\ell_k^+ + \Delta\ell - 1)d_k^+$.

Lemma 3.6. Suppose $\det(J) \neq 0$ and $\rho_{\max} < 1$. Then for any $\Delta\ell \geq 0$ there exists a neighbourhood of the \mathcal{S} -shrinking point within which $\det(P_{\mathcal{G}^+[k, \Delta\ell]}) = 0$ implies

$$f^{\mathcal{G}^+[k, \Delta\ell]}(x_{-d}^{\text{int}}) = x_{-d}^{\text{int}} + \mathcal{O}(\rho_{\max}^k), \quad (3.25)$$

where $k \in \mathbb{Z}^+$.

Proof. Suppose $\det(P_{\mathcal{G}^+[k, \Delta\ell]}) = 0$. Also suppose, for the moment, that the $\mathcal{G}^+[k, \Delta\ell]$ -cycle exists and is unique (as is generically the case, although it may not be admissible). Then $x_0^{\mathcal{G}^+[k, \Delta\ell]}$ lies on the switching manifold. Since $\rho_{\max} < 1$ and $\mathcal{G}^+[k, \Delta\ell]$ ends in a power of $\mathcal{S}^{(-d)}$ proportional to k , $x_0^{\mathcal{G}^+[k, \Delta\ell]}$ is an $\mathcal{O}(\rho_{\max}^k)$ distance from W^c (this is demonstrated formally in the proof of Lemma 7.7 of [1]). Thus $x_0^{\mathcal{G}^+[k, \Delta\ell]} = x_{-d}^{\text{int}} + \mathcal{O}(\rho_{\max}^k)$, and then (3.25) follows from the fact that $x_0^{\mathcal{G}^+[k, \Delta\ell]}$ is a fixed point of $f^{\mathcal{G}^+[k, \Delta\ell]}$.

Equation (3.25) is also true if the $\mathcal{G}^+[k, \Delta\ell]$ -cycle does not exist or is non-unique (i.e. $\det(I - M_{\mathcal{G}^+[k, \Delta\ell]}) = 0$) because the components of (3.25) are smooth functions of the parameters and $\det(I - M_{\mathcal{G}^+[k, \Delta\ell]}) \neq 0$ on a dense subset of parameter space. \square

4 An attracting invariant set

In this section we enlarge the one-dimensional fundamental domain $\Omega_{\Delta\ell} \subset W^c$ into an N -dimensional set Φ . The set Φ will have the property that iterations of any $x \in \Phi$ under f will return to Φ after following $\mathcal{G}^+[k, \Delta\ell]$, or a similar sequence, with the assumption $\rho_{\max} < 1$. For this reason Φ is referred to as a *recurrent set*.

We first define Φ in §4.1. We then study the return dynamics on Φ in §4.2 and §4.3. Lastly we use Φ to identify an attracting invariant set in §4.4.

4.1 The construction of a recurrent set

By the definition of $\Omega_{\Delta\ell}$, see (3.19), the surface

$$\left\{ x \in \mathbb{R}^N \mid e_1^\top f^{\mathcal{X}\bar{\mathcal{O}}}(\mathcal{Y}\bar{\mathcal{X}})^{\Delta\ell}(x) = 0 \right\} \quad (4.1)$$

intersects $\Omega_{\Delta\ell}$ at its right endpoint $v(h_{\Delta\ell}^R)$.

Lemma 4.1. *Suppose $\det(J) \neq 0$. Let $\Delta\ell \geq 0$ and suppose $\kappa_{\Delta\ell}^+ \neq \kappa_{\Delta\ell-1}^+$ if $\Delta\ell \geq 1$. Then (4.1) is a hyperplane not parallel to $\Omega_{\Delta\ell}$.*

Proof. By (2.3), $e_1^\top f^{\mathcal{X}\bar{\mathcal{O}}}(\mathcal{Y}\bar{\mathcal{X}})^{\Delta\ell}(x) = e_1^\top M_{\mathcal{X}\bar{\mathcal{O}}}(\mathcal{Y}\bar{\mathcal{X}})^{\Delta\ell} x + e_1^\top P_{\mathcal{X}\bar{\mathcal{O}}}(\mathcal{Y}\bar{\mathcal{X}})^{\Delta\ell} B$. This is the equation for a hyperplane with normal vector $e_1^\top M_{\mathcal{X}\bar{\mathcal{O}}}(\mathcal{Y}\bar{\mathcal{X}})^{\Delta\ell}$. By Lemma 3.4, $e_1^\top M_{\mathcal{X}\bar{\mathcal{O}}}(\mathcal{Y}\bar{\mathcal{X}})^{\Delta\ell} \zeta_{-d} \neq 0$. Thus (4.1) is a hyperplane (because the normal vector is nonzero) and is not parallel to $\Omega_{\Delta\ell}$ (because $\Omega_{\Delta\ell}$ has direction ζ_{-d}). \square

Given $k \in \mathbb{Z}^+$, $|\Delta\ell| < k$ and $Q > 0$, let

$$H_{k,\Delta\ell,Q} := \left\{ x \in \text{range}\left(f^{S^{(-d)}}\right) \mid e_1^\top f^{\mathcal{X}\bar{\mathcal{O}}}(\mathcal{Y}\bar{\mathcal{X}})^{\Delta\ell}(x) = 0, \right. \\ \left. \|(I - \zeta_{-d}\omega_{-d}^\top)(x - x_{-d}^{\text{int}})\| \leq Q\rho_{\max}^k \right\}, \quad (4.2)$$

be a subset of (4.1) that contains $v(h_{\Delta\ell}^R)$. If we write any $x \in H_{k,\Delta\ell,Q}$ in the form $x = x_{-d}^{\text{int}} + h\zeta_{-d} + q$ (3.13), then $\|q\| \leq Q\rho_{\max}^k$.

If 0 is an eigenvalue of $M_{S^{(-d)}}$, then the range of $f^{S^{(-d)}}$ has dimension less than N and the condition $H_{k,\Delta\ell,Q} \subset \text{range}\left(f^{S^{(-d)}}\right)$ is helpful below. It is tempting to ignore this complication, as it is a special case within the space of maps of the form (1.2), however it is in fact typical for 0 to be an eigenvalue of $M_{S^{(-d)}}$ in the application to grazing-sliding bifurcations [21].

Let

$$\Phi_{k,\Delta\ell,Q} := \left\{ \alpha x_1 + (1 - \alpha)x_2 \mid x_1 \in H_{k,\Delta\ell,Q}, x_2 \in f^{S^{(-d)}}(H_{k,\Delta\ell,Q}), 0 \leq \alpha < 1 \right\}. \quad (4.3)$$

For brevity we just write Φ when it is clear what values of k , $\Delta\ell$ and Q are being used. The set Φ is the convex hull of $H_{k,\Delta\ell,Q}$ and its image under $f^{S^{(-d)}}$, but not including $H_{k,\Delta\ell,Q}$. Fig. 11 shows the set Φ for two examples.

4.2 Return dynamics

Here we show that, under certain assumptions, Φ is a recurrent set for f for parameter values throughout $\Sigma_{k,\Delta\ell}^+$. Let $x \in \mathbb{R}^N$ and suppose $\rho_{\max} < 1$. Then $f^{\mathcal{G}^+[k,\Delta\ell]}(x)$ is an $\mathcal{O}(\rho_{\max}^k)$ distance from W^c (assuming $k \gg \Delta\ell$), see §3.3. Also

$$f^{\mathcal{G}^+[k+\Delta k,\Delta\ell]}(x) = f^{(S^{(-d)})^{\Delta k}}\left(f^{\mathcal{G}^+[k,\Delta\ell]}(x)\right), \quad (4.4)$$

for all $\Delta k \geq 0$ by (3.4). Moreover, (4.4) holds for all $\Delta k \geq -(k - \Delta \ell)$ where we take $\left(f^{\mathcal{S}^{(-d)}}\right)^{-1}(x)$ to be the unique inverse belonging to $\text{range}\left(f^{\mathcal{S}^{(-d)}}\right)$. Therefore $\left\{f^{\mathcal{G}^+[k+\Delta k, \Delta \ell]}(x)\right\}_{\Delta k \gg -k}$ is a sequence of points near W^c mapping from one to the next under $f^{\mathcal{S}^{(-d)}}$.

For any $y \in \text{range}\left(f^{\mathcal{S}^{(-d)}}\right)$, let $\beta(y)$ denote the smallest value of Δk for which

$$e_1^\top f^{\mathcal{X}^\circ(y^\circ \mathcal{X})^{\Delta \ell}} \left(\left(f^{\mathcal{S}^{(-d)}} \right)^{\Delta k} (y) \right) > 0, \quad (4.5)$$

and assume $\beta(y) \gg -k$. Also let

$$T(y) := \left(f^{\mathcal{S}^{(-d)}} \right)^{\beta(y)} (y). \quad (4.6)$$

Lemma 4.2. *Suppose $\det(J) \neq 0$ and $\rho_{\max} < 1$. Let $\Delta \ell \geq 0$ and suppose $\Sigma_{k, \Delta \ell}^+$ is well-defined for arbitrarily large values of k with $(\kappa_{\Delta \ell}^+ - \kappa_{\Delta \ell - 1}^+)a > 0$. If $k \in \mathbb{Z}^+$ and $Q \in \mathbb{R}$ are sufficiently large, then at any point in $\Sigma_{k, \Delta \ell}^+$ and any $x \in \Phi_{k, \Delta \ell, Q}$,*

- i) $\beta\left(f^{\mathcal{G}^+[k, \Delta \ell]}(x)\right)$ is well-defined and $f^{\mathcal{G}^+[k+\Delta k, \Delta \ell]}(x) \in \Phi$ if and only if $\Delta k = \beta\left(f^{\mathcal{G}^+[k, \Delta \ell]}(x)\right)$, and similarly
- ii) $\beta\left(f^{\mathcal{G}^+[k, \Delta \ell]^\circ}(x)\right)$ is well-defined and $f^{\mathcal{G}^+[k+\Delta k, \Delta \ell]^\circ}(x) \in \Phi$ if and only if $\Delta k = \beta\left(f^{\mathcal{G}^+[k, \Delta \ell]^\circ}(x)\right)$.

A proof of Lemma 4.2 is given in Appendix A. In Lemma 4.2 the assumption on the sign of $(\kappa_{\Delta \ell}^+ - \kappa_{\Delta \ell - 1}^+)a$ is provided as an alternative to a stronger condition of admissibility at $\mathcal{G}^+[k, \Delta \ell]$ -shrinking points and is used to show that the left hand-side of (4.5) is an increasing function of Δk .

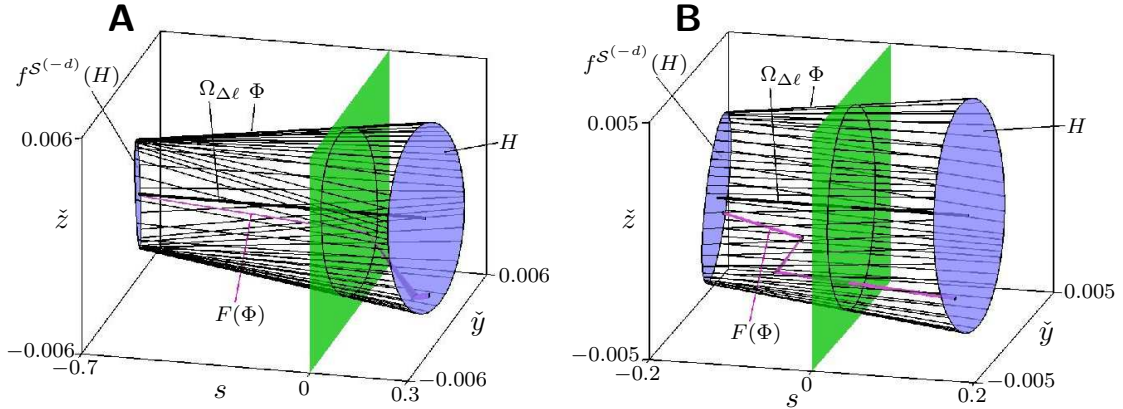


Figure 11: The recurrent set $\Phi = \Phi_{k, \Delta \ell, Q}$ (4.3) and its image under F (4.7). For clarity we have used coordinates representing the displacement from the centre manifold W^c . Panel A shows $\Phi_{2,0,0.07}$ for the parameter values of Fig. 3 with $\tau_R = -1.45$ and $\delta_L = 0.1$. Panel B shows $\Phi_{5,0,0.13}$ for the parameter values of Fig. 7 with $\tau_R = -2.12$ and $\delta_L = 0.17$. Note, the label $H_{k, \Delta \ell, Q}$ is abbreviated as H .

4.3 Continuity of the return map in a cylindrical topology

Let

$$F(x) := \begin{cases} T\left(f^{\mathcal{G}^+[k,\Delta\ell]}(x)\right), & s \leq 0, \\ T\left(f^{\mathcal{G}^+[k,\Delta\ell]^{\bar{0}}}(x)\right), & s \geq 0. \end{cases} \quad (4.7)$$

Equivalently

$$F(x) = \begin{cases} f^{\mathcal{G}^+[k+\Delta k,\Delta\ell]}(x), & s \leq 0, \\ f^{\mathcal{G}^+[k+\Delta k,\Delta\ell]^{\bar{0}}}(x), & s \geq 0, \end{cases} \quad (4.8)$$

where

$$\Delta k = \begin{cases} \beta\left(f^{\mathcal{G}^+[k,\Delta\ell]}(x)\right), & s \leq 0, \\ \beta\left(f^{\mathcal{G}^+[k,\Delta\ell]^{\bar{0}}}(x)\right), & s \geq 0. \end{cases} \quad (4.9)$$

By Lemma 4.2, $F : \Phi \rightarrow \Phi$ throughout $\Sigma_{k,\Delta\ell}^+$.

Here we *identify* the left and right faces of Φ to create a topology in which Φ is cylindrical. More specifically, we identify each $x^+ \in H_{k,\Delta\ell,Q}$ with $x^- = f^{\mathcal{S}^{(-d)}}(x^+)$.

Lemma 4.3. *The map $F : \Phi \rightarrow \Phi$ is continuous in the cylindrical topology of Φ .*

Proof. F is continuous on the switching manifold because if $s = 0$ then $f^{\mathcal{G}^+[k,\Delta\ell]}(x) = f^{\mathcal{G}^+[k,\Delta\ell]^{\bar{0}}}(x)$ by the continuity of f . Also F is continuous at any $x \in \Phi$ with $F(x) \in f^{\mathcal{S}^{(-d)}}(H_{k,\Delta\ell,Q})$, because for any small Δx the point $F(x + \Delta x)$ will lie near either $F(x)$ (if the value of $\beta(y)$ in T is unchanged) or its preimage in $H_{k,\Delta\ell,Q}$ under $f^{\mathcal{S}^{(-d)}}$ (if the value of $\beta(y)$ in T decreases by 1) and these two points are identical in the cylindrical topology of Φ .

Choose any $x^- \in f^{\mathcal{S}^{(-d)}}(H_{k,\Delta\ell,Q})$, and let x^+ be the preimage of x^- in $H_{k,\Delta\ell,Q}$ under $f^{\mathcal{S}^{(-d)}}$. It remains to show that the points

$$F(x^-) = T\left(f^{\mathcal{G}^+[k,\Delta\ell]}(x^-)\right), \quad (4.10)$$

$$F(x^+) = T\left(f^{\mathcal{G}^+[k,\Delta\ell]^{\bar{0}}}(x^+)\right), \quad (4.11)$$

are identical.

Since $x^- = f^{\mathcal{S}^{(-d)}}(x^+)$, by (3.6) we have

$$f^{\mathcal{G}^+[k,\Delta\ell]}(x^-) = f^{\mathcal{S}^{(-d)}}\left(f^{\mathcal{G}^+[k,\Delta\ell]^{\bar{0}}}\left(\overline{(\ell_k^+ + \Delta\ell)_{d_k^+}}(x^+)\right)\right).$$

Since $x^+ \in H_{k,\Delta\ell,Q}$, by the continuity of f this is the same as

$$f^{\mathcal{G}^+[k,\Delta\ell]}(x^-) = f^{\mathcal{S}^{(-d)}}\left(f^{\mathcal{G}^+[k,\Delta\ell]^{\bar{0}}}(x^+)\right).$$

Therefore (4.10) can be rewritten as

$$F(x^-) = T\left(f^{\mathcal{S}^{(-d)}}\left(f^{\mathcal{G}^+[k,\Delta\ell]^{\bar{0}}}(x^+)\right)\right),$$

which is identical to (4.11) because $T \circ f^{\mathcal{S}^{(-d)}} = T$ by the definition of T . □

4.4 An attracting invariant set and its topology

Fig. 11 shows the set $F(\Phi)$ for two examples. If we continue to iterate Φ under F we obtain the attracting invariant set

$$\Lambda_{\Delta\ell} := \bigcap_{i=0}^{\infty} F^i(\Phi). \quad (4.12)$$

Lemma 4.4. *The sets $\Lambda_{\Delta\ell}$ and $\Omega_{\Delta\ell}$ are homotopic in the cylindrical topology of Φ .*

Roughly speaking this means that $\Lambda_{\Delta\ell}$ can be transformed to $\Omega_{\Delta\ell}$ by distorting it in a continuous fashion [22, 23]. Below we prove Lemma 4.4 by using the following result.

Lemma 4.5. *Let $\Psi \subset \Phi$ be connected. If $F(\Psi) \subset \Psi$, then Ψ and $F(\Psi)$ are homotopic in the cylindrical topology of Φ .*

To say that Ψ and $F(\Psi)$ are *homotopic* means that there exists a continuous function $K : \Phi \times [0, 1] \rightarrow \Phi$ with $K(x, 0) = x$ and $K(x, 1) = F(x)$ for all $x \in \Psi$. The function K is said to be a *homotopy* between ι_{Ψ} (the inclusion of Ψ) and $F|_{\Psi}$ (the restriction of F to Ψ).

Proof of Lemma 4.5. Define $K : \Phi \times [0, 1] \rightarrow \Phi$ by

$$K(x, \alpha) := \begin{cases} T\left((1 - \alpha)x + \alpha f^{\mathcal{G}^+[k, \Delta\ell]}(x)\right), & s \leq 0, \\ T\left((1 - \alpha)x + \alpha f^{\mathcal{G}^+[k, \Delta\ell]^{\bar{0}}}(x)\right), & s \geq 0. \end{cases} \quad (4.13)$$

By (4.6), $K(x, 0) = x$ for all $x \in \Psi$. Also, by (4.7), $K(x, 1) = F(x)$ for all $x \in \Psi$.

Choose any $x^- \in f^{\mathcal{S}^{(-d)}}(H_{k, \Delta\ell, Q})$, and let x^+ be the preimage of x^- in $H_{k, \Delta\ell, Q}$ under $f^{\mathcal{S}^{(-d)}}$. We wish to show that

$$K(x^-, \alpha) = T\left((1 - \alpha)x^- + \alpha f^{\mathcal{G}^+[k, \Delta\ell]}(x^-)\right), \quad (4.14)$$

$$K(x^+, \alpha) = T\left((1 - \alpha)x^+ + \alpha f^{\mathcal{G}^+[k, \Delta\ell]^{\bar{0}}}(x^+)\right), \quad (4.15)$$

are identical for all $\alpha \in [0, 1]$. Following the steps of the proof of Lemma 4.3, we obtain

$$K(x^-, \alpha) = T\left((1 - \alpha)f^{\mathcal{S}^{(-d)}}(x^+) + \alpha f^{\mathcal{S}^{(-d)}}\left(f^{\mathcal{G}^+[k, \Delta\ell]^{\bar{0}}}(x^+)\right)\right).$$

Since $f^{\mathcal{S}^{(-d)}}$ is affine, this is the same as

$$K(x^-, \alpha) = T\left(f^{\mathcal{S}^{(-d)}}\left((1 - \alpha)x^+ + \alpha f^{\mathcal{G}^+[k, \Delta\ell]^{\bar{0}}}(x^+)\right)\right),$$

which is identical to (4.15) because $T \circ f^{\mathcal{S}^{(-d)}} = T$.

This shows that K is continuous at any $x^- \in f^{\mathcal{S}^{(-d)}}(H_{k, \Delta\ell, Q})$. As with F , the function K is continuous on the switching manifold and at any $x \in \Phi$ with $K(x, \alpha) \in f^{\mathcal{S}^{(-d)}}(H_{k, \Delta\ell, Q})$. Thus K is continuous throughout Φ for any $\alpha \in [0, 1]$. Thus K is indeed a homotopy and hence Ψ and $F(\Psi)$ are homotopic. \square

Proof of Lemma 4.4. By applying Lemma 4.5 to $\Psi = \Phi$, $\Psi = F(\Phi)$, $\Psi = F^2(\Phi)$, and so on, we deduce that Φ and $\Lambda_{\Delta\ell}$ are homotopic. It is clear that $\Omega_{\Delta\ell}$ and Φ are homotopic in view of the definition of Φ , thus $\Lambda_{\Delta\ell}$ and $\Omega_{\Delta\ell}$ are homotopic. \square

5 The skew sawtooth map as an approximate return map

5.1 One-dimensional approximation

Recall, for any $x \in \mathbb{R}^N$ written as $x = x_{-d}^{\text{int}} + h\zeta_{-d} + q$ (3.13), the function $u(x)$ extracts the value of h , and for any $h \in \mathbb{R}$ the function $v(h)$ returns the point $x_{-d}^{\text{int}} + h\zeta_{-d} \in W^c$. Thus for any $x \in W^c$ we have $v(u(x)) = x$ and for any x near W^c we have $v(u(x)) \approx x$.

The set $\Phi = \Phi_{k,\Delta\ell,Q}$ is an $\mathcal{O}(\rho_{\max}^k)$ fattening of the fundamental domain $\Omega_{\Delta\ell} \subset W^c$. Thus for any $x \in \Phi$ we have $v(u(x)) \approx x$ and $v(u(F(x))) \approx F(x)$ because $F(x) \in \Phi$. In this way the N -dimensional map F is well-approximated by the one-dimensional map taking $u(x)$ to $u(F(x))$. This is the map

$$G := u \circ F \circ v. \quad (5.1)$$

The map G is piecewise-linear but over the interval $[h_{\Delta\ell}^L, h_{\Delta\ell}^R)$ can involve many different linear pieces corresponding to different values of Δk . Next we show that, with fixed values of $\Delta\ell$ and θ , the leading order components of the slopes of these pieces only take two different values.

Lemma 5.1. *Suppose $\det(J) \neq 0$ and $\rho_{\max} < 1$. Let $\Delta\ell \geq 0$ and suppose $\Sigma_{k,\Delta\ell}^+$ is well-defined for arbitrarily large values of k with $(\kappa_{\Delta\ell}^+ - \kappa_{\Delta\ell-1}^+)a > 0$. Then at any point in $\Sigma_{k,\Delta\ell}^+$ and any $h \in \mathbb{R}$,*

$$\frac{d}{dh} u\left(f^{\mathcal{G}^+[k,\Delta\ell]}(v(h))\right) = \frac{t_{-d}\kappa_{\Delta\ell}^+ \tan(\theta)}{t_d} + \mathcal{O}\left(\frac{1}{k}\right), \quad (5.2)$$

$$\frac{d}{dh} u\left(f^{\mathcal{G}^+[k,\Delta\ell]^{\bar{0}}}(v(h))\right) = \begin{cases} \frac{t_{(\ell-1)d}\kappa_{-1}^+ \tan(\theta)}{t_{(\ell+1)d}} + \mathcal{O}\left(\frac{1}{k}\right), & \Delta\ell = 0, \\ \frac{t_{-d}\kappa_{\Delta\ell-1}^+ \tan(\theta)}{t_d} + \mathcal{O}\left(\frac{1}{k}\right), & \Delta\ell \geq 1, \end{cases} \quad (5.3)$$

where $k \in \mathbb{Z}^+$.

Lemma 5.1 is proved in Appendix A. Since G is given by (5.1), where F is equal to $f^{\mathcal{G}^+[k+\Delta k,\Delta\ell]}$ or $f^{\mathcal{G}^+[k+\Delta k,\Delta\ell]^{\bar{0}}}$ for some $\mathcal{O}(1)$ value of Δk , the slopes of G are given by (5.2) and (5.3) to leading order.

5.2 Circle map formulation

The function

$$\varphi(h) := \begin{cases} \frac{h-h_{\Delta\ell}^L}{h_{\Delta\ell}^R-h_{\Delta\ell}^L}, & a < 0, \\ \frac{-h}{h_{\Delta\ell}^R-h_{\Delta\ell}^L} \bmod 1, & a > 0. \end{cases} \quad (5.4)$$

transforms the interval $[h_{\Delta\ell}^L, h_{\Delta\ell}^R)$ into $[0, 1)$ (the domain of the skew sawtooth map (1.5)). We use this particular a -dependent transformation because it leads to convenient a -independent formulas for w and Δk .

Theorem 5.2. *Suppose $\det(J) \neq 0$ and $\rho_{\max} < 1$. Let $\Delta\ell \geq 0$ and suppose $\Sigma_{k,\Delta\ell}^+$ is well-defined for arbitrarily large values of k with $(\kappa_{\Delta\ell}^+ - \kappa_{\Delta\ell-1}^+)a > 0$. Let $\theta_{\min} = \min(\theta_{\Delta\ell}^+, \theta_{\Delta\ell-1}^+)$*

and $\theta_{\max} = \max(\theta_{\Delta\ell}^+, \theta_{\Delta\ell-1}^+)$. Then at any point in $\Sigma_{k,\Delta\ell}^+$, there exists $\Xi \subset \Phi$ with $\frac{\text{meas}(\Xi)}{\text{meas}(\Phi)} = \mathcal{O}(\frac{1}{k})$ such that throughout $\Phi \setminus \Xi$,

$$F = v \circ \varphi^{-1} \circ g \circ \varphi \circ u + \mathcal{O}\left(\frac{1}{k^2}\right), \quad (5.5)$$

where g is given by (1.5) with

$$a_L = \begin{cases} \frac{\tan(\theta)}{\tan(\theta_{\min})}, & \kappa_{\Delta\ell}^+ > 0, \kappa_{\Delta\ell-1}^+ > 0, \\ -\frac{\tan(\theta)}{\tan(\theta_{\min})}, & \kappa_{\Delta\ell}^+ \kappa_{\Delta\ell-1}^+ < 0, \end{cases} \quad a_R = \frac{\tan(\theta)}{\tan(\theta_{\max})}, \quad w = k^2 \delta. \quad (5.6)$$

Moreover, for any $x \in \Phi \setminus \Xi$,

$$F(x) = \begin{cases} f^{\mathcal{G}^+[k+\Delta k, \Delta\ell]}(x), & 0 \leq z \leq z_{\text{sw}}, \\ f^{\mathcal{G}^+[k+\Delta k, \Delta\ell]^{\bar{0}}}(x), & z_{\text{sw}} \leq z < 1, \end{cases} \quad (5.7)$$

where $\Delta k = g_{\text{lift}}(z) - g(z)$ and $z = \varphi(u(x))$.

Theorem 5.2 explicitly indicates how g (1.5) approximates the dynamics of f (1.2). Specifically, g can be used to approximate the return map F via the formula (5.5), where the parameters of g are given by (5.6) and the relationship of F to f is given by (5.7). For $x \in \Xi$, either $u(x) \notin \Omega_{\Delta\ell}$, in which case (5.5) is not well-defined, or $F(x)$ corresponds to a different sequence of iterates of f than that given by (5.7). These discrepancies have not been seen to cause qualitatively different dynamics for f and g because these are continuous maps and Ξ constitutes a vanishingly small fraction of Φ as $k \rightarrow \infty$.

6 Discussion

This paper continues the work of [1] to rigorously characterise the dynamics of (1.2) near an \mathcal{S} -shrinking point (where $\mathcal{S} = \mathcal{F}[\ell, m, n]$). Relative to the distance from an \mathcal{S} -shrinking point, of all nearby mode-locking regions the \mathcal{G}_k^\pm -mode-locking regions are the largest. This is because, symbolically, they belong to the first level of complexity relative to \mathcal{S} . The \mathcal{G}_k^\pm -mode-locking regions, and their shrinking points, were analysed in [1]. The results of the present paper help explain the dynamics that occurs between the \mathcal{G}_k^\pm -mode-locking regions: higher period solutions, quasiperiodic dynamics, and chaos.

We have shown that such dynamics is captured by a skew sawtooth map (1.5) with three parameters: the slopes a_L and a_R , and the vertical displacement w . To relate (1.2) to (1.5) quantitatively, we defined an array of sectors $\Sigma_{k,\Delta\ell}^\pm$ near the \mathcal{S} -shrinking point. Within each $\Sigma_{k,\Delta\ell}^\pm$ the dynamics of (1.2) is well-approximated by that of (1.5) with fixed formulas for a_L , a_R and w in terms of (δ, θ) -coordinates. We identified a region Φ to which forward orbits regularly return, and considered the first return map $F : \Phi \rightarrow \Phi$ that equals the composition of (1.2) with itself many times (proportional to kn). Theorem 5.2 indicates precisely how (1.5) can be used to approximate F .

The results of §4.4 describe the nature of the attracting invariant set $\Lambda_{\Delta\ell}$ on which the dynamics is well approximated by (1.5). By Lemma 4.4, $\Lambda_{\Delta\ell}$ is homotopic to a loop with a

cylindrical topology on Φ . This tells us that the invariant set $\cup_{i \geq 0} f^i(\Lambda_{\Delta\ell})$ of (1.2) is either an invariant loop or a complicated geometric object that is homotopic to an invariant loop in \mathbb{R}^N .

For the map (1.5), the value of w varies linearly from 0 to 1 as we move from the outer boundary of $\Sigma_{k,\Delta\ell}^\pm$ to the inner boundary of $\Sigma_{k,\Delta\ell}^\pm$, and so is given by $w = k^2\delta$. Lemma 5.1 essentially tells us that the slopes a_L and a_R are proportional to λ^k , where λ is the critical eigenvalue of M_S (that is, $\lambda = 1$ at the \mathcal{S} -shrinking point). By equations (7.43)–(7.44) of [1], in $\Sigma_{k,\Delta\ell}^+$ we have $\lambda^k = \tan(\theta) + \mathcal{O}(\frac{1}{k})$, whereas in $\Sigma_{k,\Delta\ell}^-$ we have $\lambda^k = \frac{1}{\tan(\theta)} + \mathcal{O}(\frac{1}{k})$. The slopes a_L and a_R are also such that $a_R = 1$ on one of the two linear boundaries of $\Sigma_{k,\Delta\ell}^\pm$ and either $a_L = 1$ or $a_L = -1$ on the other linear boundary of $\Sigma_{k,\Delta\ell}^\pm$, see Table 1.

The dynamics in $\Sigma_{k,\Delta\ell}^\pm$ corresponds to a two-dimensional cross-section of the three-dimensional parameter space of (1.5) as characterised by the value of $\frac{a_R}{a_L}$ (which is constant throughout $\Sigma_{k,\Delta\ell}^\pm$). Qualitatively, there are two distinct scenarios as determined by the sign of $\frac{a_R}{a_L}$. If $\frac{a_R}{a_L} > 0$, then (1.5) is a homeomorphism and has a unique rotation number. Periodic dynamics occurs within mode-locking regions that exhibit shrinking points and non-periodic dynamics is quasiperiodic. The value of $\frac{a_R}{a_L}$ dictates the overall fatness of the mode-locking regions, see Fig. 5. This explains the presence of the roughly horizontal strip in the left half of Fig. 3 where mode-locking regions are relatively sparse. Here $\mathcal{G}^+[k, 0]$ and $\mathcal{G}^+[k, 1]$ -shrinking points are relatively close together, hence $\theta_0^+ - \theta_1^+$ is relatively small. For sectors between these two sequences of shrinking points we have $\theta_{\min} = \theta_1^+$ and $\theta_{\max} = \theta_0^+$, thus the value of $\frac{a_R}{a_L} = \frac{\tan(\theta_{\min})}{\tan(\theta_{\max})}$ is relatively small and so the mode-locking regions are relatively narrow. It remains to quantify this observation by calculating, say, the fraction of the parameter space of (1.5), with $\frac{a_R}{a_L} > 0$ fixed, for which (1.5) has a rational rotation number.

If $\frac{a_R}{a_L} < 0$, then (1.5) is not invertible. There may be coexisting attractors and chaotic dynamics [17]. Mode-locking regions do not have shrinking points but rather terminate due to a loss of stability by attaining a stability multiplier of -1 . It remains to further understand these dynamics to explain how curves connecting shrinking points can form a boundary for chaotic dynamics, as identified numerically in [24].

A Additional proofs

Proof of Lemma 3.5. For brevity we derive (3.23) and (3.24) only for $\Delta\ell \geq 1$. The result for $\Delta\ell = 0$ can be obtained in a similar fashion (and is a little simpler).

By (3.15) and (3.18),

$$h_{\Delta\ell}^L = s_{-d}^{\text{step}} + h_{\Delta\ell}^R \lambda. \quad (\text{A.1})$$

Then (3.23) is obtained by combining (3.24), $\lambda = 1 + \mathcal{O}(\eta, \nu)$, and equation (A.9) of [1]:

$$s_{-d}^{\text{step}} = \frac{at_{-d}}{ct_{(\ell-1)d}} \nu + \mathcal{O}((\eta, \nu)^2). \quad (\text{A.2})$$

It therefore just remains for us to derive (3.24).

We begin by manipulating the numerator of (3.20), where $\{x_i^{\mathcal{S}^{\overline{td}}}\}$ denotes the unique $\mathcal{S}^{\overline{td}}$ -

cycle:

$$\begin{aligned}
e_1^\top f^{\mathcal{X}\bar{\mathcal{Y}}(\mathcal{Y}\bar{\mathcal{Y}}\mathcal{X})^{\Delta\ell}}(x_{-d}^{\text{int}}) &= e_1^\top f^{\mathcal{X}(\mathcal{Y}\bar{\mathcal{Y}}\mathcal{X})^{\Delta\ell}}(x_{-d}^{\text{int}}) \\
&= e_1^\top f^{(\mathcal{S}^{\bar{\ell}\bar{d}})^{\Delta\ell}}\mathcal{X}(x_{-d}^{\text{int}}) \\
&= e_1^\top f^{(\mathcal{S}^{\bar{\ell}\bar{d}})^{\Delta\ell}}\mathcal{X}(x_0^{\mathcal{S}^{\bar{\ell}\bar{d}}}) + e_1^\top M_{(\mathcal{S}^{\bar{\ell}\bar{d}})^{\Delta\ell}\mathcal{X}}(x_{-d}^{\text{int}} - x_0^{\mathcal{S}^{\bar{\ell}\bar{d}}}) \\
&= e_1^\top f^{\mathcal{X}}(x_0^{\mathcal{S}^{\bar{\ell}\bar{d}}}) + e_1^\top M_{\mathcal{X}}M_{\mathcal{S}^{\bar{\ell}\bar{d}}}^{\Delta\ell}(x_{-d}^{\text{int}} - x_0^{\mathcal{S}^{\bar{\ell}\bar{d}}}) \\
&= s_{\ell d}^{\mathcal{S}^{\bar{\ell}\bar{d}}} + e_1^\top M_{\mathcal{X}}M_{\mathcal{S}^{\bar{\ell}\bar{d}}}^{\Delta\ell}(x_{-d}^{\text{int}} - x_0^{\mathcal{S}^{\bar{\ell}\bar{d}}}). \tag{A.3}
\end{aligned}$$

In a neighbourhood of the \mathcal{S} -shrinking point, one component of its corresponding mode-locking region is where $\eta \geq 0$ and $\nu \geq 0$, while the other component is where $\eta \leq \psi_1(\nu)$ and $\nu \leq \psi_2(\eta)$, for some C^K functions ψ_1 and ψ_2 with $\psi_1(0) = \psi_1'(0) = \psi_2(0) = \psi_2'(0) = 0$, see Theorem 6.9 of [1].

First suppose $\eta = \psi_1(\nu)$. Then $s_{\ell d}^{\mathcal{S}^{\bar{\ell}\bar{d}}} = 0$ and so by (A.3) the numerator of (3.20) is

$$e_1^\top f^{\mathcal{X}\bar{\mathcal{Y}}(\mathcal{Y}\bar{\mathcal{Y}}\mathcal{X})^{\Delta\ell}}(x_{-d}^{\text{int}}) = e_1^\top M_{\mathcal{X}}M_{\mathcal{S}^{\bar{\ell}\bar{d}}}^{\Delta\ell}(x_{-d}^{\text{int}} - x_0^{\mathcal{S}^{\bar{\ell}\bar{d}}}). \tag{A.4}$$

By (3.22),

$$e_1^\top M_{\mathcal{X}}M_{\mathcal{S}^{\bar{\ell}\bar{d}}}^{\Delta\ell}|_{(\eta,\nu)=(0,0)} = \frac{ct_{(\ell+1)d}}{bt_d} u_0^\top M_{\mathcal{S}^{\bar{\ell}\bar{d}}}^{\Delta\ell}(I - M_{\mathcal{S}^{\bar{\ell}\bar{d}}})|_{(\eta,\nu)=(0,0)}. \tag{A.5}$$

Since $x_0^{\mathcal{S}^{\bar{\ell}\bar{d}}}$ is a fixed point of $f^{\mathcal{S}^{\bar{\ell}\bar{d}}}$, we have $x_0^{\mathcal{S}^{\bar{\ell}\bar{d}}} = (I - M_{\mathcal{S}^{\bar{\ell}\bar{d}}})^{-1} P_{\mathcal{S}^{\bar{\ell}\bar{d}}} B \mu$, from which we obtain

$$\begin{aligned}
(I - M_{\mathcal{S}^{\bar{\ell}\bar{d}}})(x_{-d}^{\text{int}} - x_0^{\mathcal{S}^{\bar{\ell}\bar{d}}}) &= (I - M_{\mathcal{S}^{\bar{\ell}\bar{d}}})x_{-d}^{\text{int}} - P_{\mathcal{S}^{\bar{\ell}\bar{d}}} B \mu \\
&= x_{-d}^{\text{int}} - (M_{\mathcal{S}^{\bar{\ell}\bar{d}}} x_{-d}^{\text{int}} + P_{\mathcal{S}^{\bar{\ell}\bar{d}}} B \mu) \\
&= x_{-d}^{\text{int}} - f^{\mathcal{S}^{\bar{\ell}\bar{d}}}(x_{-d}^{\text{int}}) \\
&= -s_{-d}^{\text{step}} \zeta_{-d}, \tag{A.6}
\end{aligned}$$

using also (3.15) in the last line. By combining (2.13), (A.2), (A.4), (A.5), (A.6) and the formula for $\kappa_{\Delta\ell}^+$ given in Appendix B, we obtain

$$e_1^\top f^{\mathcal{X}\bar{\mathcal{Y}}(\mathcal{Y}\bar{\mathcal{Y}}\mathcal{X})^{\Delta\ell}}(x_{-d}^{\text{int}}) = \kappa_{\Delta\ell}^+ \nu + \mathcal{O}(\nu^2), \tag{A.7}$$

under the assumption $\eta = \psi_1(\nu)$.

Now suppose $\nu = \psi_2(\eta)$. Then $s_0^{\mathcal{S}^{\bar{\ell}\bar{d}}} = 0$ and the \mathcal{S} -cycle is unique with $x_i^{\mathcal{S}} = x_{i+d}^{\mathcal{S}^{\bar{\ell}\bar{d}}}$, for each i . Thus by (3.10),

$$x_{-d}^{\text{int}} = (I - \zeta_{-d} e_1^\top) x_0^{\mathcal{S}^{\bar{\ell}\bar{d}}} = x_0^{\mathcal{S}^{\bar{\ell}\bar{d}}}. \tag{A.8}$$

The numerator of (3.20) is then

$$\begin{aligned}
e_1^\top f^{\mathcal{X}\bar{0}}(y^{\bar{0}}\mathcal{X})^{\Delta_\ell}(x_{-d}^{\text{int}}) &= e_1^\top f^{\mathcal{X}}(y^{\bar{0}}\mathcal{X})^{\Delta_\ell}(x_0^{\mathcal{S}^{\bar{t}d}}) \\
&= e_1^\top f^{\mathcal{X}}(x_0^{\mathcal{S}^{\bar{t}d}}) \\
&= e_1^\top x_{\ell d}^{\mathcal{S}^{\bar{t}d}} \\
&= s_{\ell d}^{\mathcal{S}^{\bar{t}d}} \\
&= \frac{t_{(\ell-1)d}}{t_{-d}}\eta + \mathcal{O}(\eta^2),
\end{aligned} \tag{A.9}$$

where in the last step we have used (2.13) and equation (58) of [19].

By combining (A.7) and (A.9) we obtain

$$e_1^\top f^{\mathcal{X}\bar{0}}(y^{\bar{0}}\mathcal{X})^{\Delta_\ell}(x_{-d}^{\text{int}}) = \frac{t_{(\ell-1)d}}{t_{-d}}\eta + \kappa_{\Delta\ell}^+\nu + \mathcal{O}((\eta, \nu)^2). \tag{A.10}$$

Then (3.24) is given by (A.10) divided by (3.21). \square

Proof of Lemma 4.2. For brevity we prove the result only for $\mathcal{G}^+[k, \Delta\ell]$. The result for $\mathcal{G}^+[k, \Delta\ell]^{\bar{0}}$ can be proved in the same fashion.

Step 1. We first use Lemma 3.4 to show that

$$e_1^\top M_{\mathcal{X}\bar{0}}(y^{\bar{0}}\mathcal{X})^{\Delta_\ell}\zeta_{-d} < 0, \tag{A.11}$$

throughout $\Sigma_{k, \Delta\ell}^+$.

At the \mathcal{S} -shrinking point the $\mathcal{S}^{\bar{0}}$ -cycle, denoted $\{y_i\}$, is assumed to be admissible with only y_0 and $y_{\ell d}$ on the switching manifold. Therefore $t_{(\ell-1)d} < 0$ and $t_{-d} > 0$. Since $\rho_{\max} < 1$, we have $c > 0$. Also $(\kappa_{\Delta\ell}^+ - \kappa_{\Delta\ell-1}^+)a > 0$ by assumption. By applying these inequalities to (3.21) we obtain (A.11).

Step 2. Next we show that $h_{\Delta\ell}^L < h_{\Delta\ell}^R$.

From now on we only consider parameter values in $\Sigma_{k, \Delta\ell}^+$. Then $\text{sgn}(\nu) = \text{sgn}(a)$, see §2.3. Also η and ν are $\mathcal{O}(\frac{1}{k})$. Thus, by (A.2), $s_{-d}^{\text{step}} < 0$ for sufficiently large values of k .

By (3.11), (3.18), and (3.15),

$$h_{\Delta\ell}^L = s_{-d}^{\text{step}} + h_{\Delta\ell}^R\lambda. \tag{A.12}$$

Since $s_{-d}^{\text{step}} = \mathcal{O}(\frac{1}{k})$, $\lambda = 1 + \mathcal{O}(\frac{1}{k})$, and $h_{\Delta\ell}^L$ and $h_{\Delta\ell}^R$ are $\mathcal{O}(\frac{1}{k})$ by (3.23)–(3.24), we have

$$h_{\Delta\ell}^R - h_{\Delta\ell}^L = -s_{-d}^{\text{step}} + \mathcal{O}\left(\frac{1}{k^2}\right). \tag{A.13}$$

Therefore $h_{\Delta\ell}^L < h_{\Delta\ell}^R$ (throughout $\Sigma_{k, \Delta\ell}^+$) for sufficiently large values of k .

Step 3. We have thus shown that $\Omega_{\Delta\ell}$ is well-defined by (3.19). Moreover, $\Omega_{\Delta\ell}$ is an $\mathcal{O}(\frac{1}{k})$ distance from the switching manifold, and so is Φ . In this step we show that $f^{\mathcal{G}^+[k, \Delta\ell]}(\Phi)$ is also an $\mathcal{O}(\frac{1}{k})$ distance from the switching manifold.

On the outer boundary of $\Sigma_{k,\Delta\ell}^+$, the matrix $P_{\mathcal{G}^+[k,\Delta\ell](i)}$ is singular for either $i = 0$ or $i = (\ell_k^+ + \Delta\ell - 1)d_k^+$. For brevity we just treat the case $i = 0$. Then by (3.25), on the outer boundary of $\Sigma_{k,\Delta\ell}^+$ the point $f^{\mathcal{G}^+[k,\Delta\ell]}(x_{-d}^{\text{int}})$ is an $\mathcal{O}(\rho_{\max}^k)$ distance from the switching manifold.

In order to describe $f^{\mathcal{G}^+[k,\Delta\ell]}(x_{-d}^{\text{int}})$ for parameter values on the inner boundary of $\Sigma_{k,\Delta\ell}^+$, we first note that on this boundary $P_{\mathcal{G}^+[k+1,\Delta\ell]}$ is singular. Thus by (3.25)

$$f^{\mathcal{G}^+[k+1,\Delta\ell]}(x_{-d}^{\text{int}}) = x_{-d}^{\text{int}} + \mathcal{O}(\rho_{\max}^k). \quad (\text{A.14})$$

By (4.4), $f^{\mathcal{G}^+[k,\Delta\ell]}(x_{-d}^{\text{int}})$ is the unique inverse of $f^{\mathcal{G}^+[k+1,\Delta\ell]}(x_{-d}^{\text{int}})$ under $f^{\mathcal{S}^{(-d)}}$ that belongs to the range of $f^{\mathcal{S}^{(-d)}}$. Thus by (3.15)

$$f^{\mathcal{G}^+[k,\Delta\ell]}(x_{-d}^{\text{int}}) = x_{-d}^{\text{int}} - \frac{s_{-d}^{\text{step}}}{\lambda} \zeta_{-d} + \mathcal{O}(\rho_{\max}^k), \quad (\text{A.15})$$

on the inner boundary of $\Sigma_{k,\Delta\ell}^+$. Therefore $f^{\mathcal{G}^+[k,\Delta\ell]}(x_{-d}^{\text{int}})$ is an $\mathcal{O}(\frac{1}{k})$ distance from the switching manifold on the inner boundary of $\Sigma_{k,\Delta\ell}^+$. It follows that $f^{\mathcal{G}^+[k,\Delta\ell]}(x_{-d}^{\text{int}})$ is an $\mathcal{O}(\frac{1}{k})$ distance from the switching manifold throughout $\Sigma_{k,\Delta\ell}^+$.

Now we show that for any $x \in \Phi$ we have

$$f^{\mathcal{G}^+[k,\Delta\ell]}(x) - f^{\mathcal{G}^+[k,\Delta\ell]}(x_{-d}^{\text{int}}) = \mathcal{O}\left(\frac{1}{k}\right), \quad (\text{A.16})$$

which will complete our demonstration that $f^{\mathcal{G}^+[k,\Delta\ell]}(\Phi)$ is an $\mathcal{O}(\frac{1}{k})$ distance from the switching manifold. In view of (3.4), since $x - x_{-d}^{\text{int}} = \mathcal{O}(\frac{1}{k})$ we have $f^{(\mathcal{X}\mathcal{Y}^{\bar{0}})^{\Delta\ell}\hat{\mathcal{X}}}(x) - f^{(\mathcal{X}\mathcal{Y}^{\bar{0}})^{\Delta\ell}\hat{\mathcal{X}}}(x_{-d}^{\text{int}}) = \mathcal{O}(\frac{1}{k})$ because $f^{(\mathcal{X}\mathcal{Y}^{\bar{0}})^{\Delta\ell}\hat{\mathcal{X}}}$ is independent of k . Since $\rho_{\max} < 1$, all eigenvalues of the matrix part of $f^{\mathcal{S}^{(-d)}}$ have modulus less than 1 except possibly λ . But $\lambda^k = \mathcal{O}(1)$ because $\lambda = 1 + \mathcal{O}(\eta, \nu)$ and η and ν are $\mathcal{O}(\frac{1}{k})$. Therefore $(f^{\mathcal{S}^{(-d)}})^{k-\Delta\ell}$ is not expanding by more than an $\mathcal{O}(1)$ factor, which verifies (A.16) by (3.4).

Step 4. Next we show that $\beta(y)$ is well-defined with $y = f^{\mathcal{G}^+[k,\Delta\ell]}(x)$ and any $x \in \Phi$.

For any $y = v(h) \in W^c$, by (3.15) we have

$$\begin{aligned} e_1^\top f^{\mathcal{X}^{\bar{0}}(\mathcal{Y}^{\bar{0}}\mathcal{X})^{\Delta\ell}}(f^{\mathcal{S}^{(-d)}}(y)) - e_1^\top f^{\mathcal{X}^{\bar{0}}(\mathcal{Y}^{\bar{0}}\mathcal{X})^{\Delta\ell}}(y) &= e_1^\top M_{\mathcal{X}^{\bar{0}}(\mathcal{Y}^{\bar{0}}\mathcal{X})^{\Delta\ell}}(f^{\mathcal{S}^{(-d)}}(y) - y) \\ &= (s_{-d}^{\text{step}} + (\lambda - 1)h) e_1^\top M_{\mathcal{X}^{\bar{0}}(\mathcal{Y}^{\bar{0}}\mathcal{X})^{\Delta\ell}} \zeta_{-d}. \end{aligned} \quad (\text{A.17})$$

Since $s_{-d}^{\text{step}} < 0$, by (A.11) we have that (A.17) is negative for sufficiently small values of h . Moreover, since s_{-d}^{step} and $(\lambda - 1)$ are $\mathcal{O}(\frac{1}{k})$, (A.17) is negative if $h = \mathcal{O}(\frac{1}{k})$, and this is also true for points y sufficiently close to W^c .

For any $x \in \Phi$, $f^{\mathcal{G}^+[k,\Delta\ell]}(x)$ is an $\mathcal{O}(\frac{1}{k})$ distance from the switching manifold and an $\mathcal{O}(\rho_{\max}^k)$ distance from W^c , and the same is true for $f^{\mathcal{G}^+[k+\Delta k,\Delta\ell]}(x)$ with $\Delta k = \mathcal{O}(1)$. This shows that (A.17) is negative using $y = f^{\mathcal{G}^+[k+\Delta k,\Delta\ell]}(x)$. Therefore the left hand-side of (4.5) is an increasing function of Δk . Thus $\beta(y)$ is well-defined.

Step 5. Now we show that if $\Delta k = \beta(f^{\mathcal{G}^+[k,\Delta\ell]}(x))$ for some $x \in \Phi$, then $f^{\mathcal{G}^+[k+\Delta k,\Delta\ell]}(x) \in \Phi$.

Let ω_{-d}^\perp denote the orthogonal complement of ω_{-d} . We define a function $\psi : \omega_{-d}^\perp \rightarrow \mathbb{R}$ by

$$\psi(q) := h_{\Delta\ell}^R - \frac{e_1^\top M_{\mathcal{X}^\top(\mathcal{Y}^\top \mathcal{X})^{\Delta\ell}} q}{e_1^\top M_{\mathcal{X}^\top(\mathcal{Y}^\top \mathcal{X})^{\Delta\ell}} \zeta_{-d}}. \quad (\text{A.18})$$

Given any $q \in \omega_{-d}^\perp$, let $x = x_{-d}^{\text{int}} + \psi(q)\zeta_{-d} + q$. It is straight-forward to show that $e_1^\top f^{\mathcal{X}^\top(\mathcal{Y}^\top \mathcal{X})^{\Delta\ell}}(x) = 0$. Thus if q is sufficiently small and $x \in \text{range}(f^{\mathcal{S}^{(-d)}})$, then $x \in H_{k,\Delta\ell,Q}$.

Choose any $x \in \Phi$ and let $\Delta k = \beta(f^{\mathcal{G}^+[k,\Delta\ell]}(x))$. By the definition of β we have

$$e_1^\top f^{\mathcal{X}^\top(\mathcal{Y}^\top \mathcal{X})^{\Delta\ell}}(f^{\mathcal{G}^+[k+\Delta k,\Delta\ell]}(x)) > 0, \quad (\text{A.19})$$

$$e_1^\top f^{\mathcal{X}^\top(\mathcal{Y}^\top \mathcal{X})^{\Delta\ell}}(f^{\mathcal{G}^+[k+\Delta k-1,\Delta\ell]}(x)) \leq 0. \quad (\text{A.20})$$

Write $f^{\mathcal{G}^+[k+\Delta k,\Delta\ell]}(x) = x_{-d}^{\text{int}} + h\zeta_{-d} + q$. Let $h_1 = \psi(q)$ and $x_1 = x_{-d}^{\text{int}} + h_1\zeta_{-d} + q$. Then $x_1 \in H_{k,\Delta\ell,Q}$, assuming Q is sufficiently large. Moreover,

$$e_1^\top f^{\mathcal{X}^\top(\mathcal{Y}^\top \mathcal{X})^{\Delta\ell}}(f^{\mathcal{G}^+[k+\Delta k,\Delta\ell]}(x)) = (h - h_1)e_1^\top M_{\mathcal{X}^\top(\mathcal{Y}^\top \mathcal{X})^{\Delta\ell}} \zeta_{-d},$$

thus $h < h_1$ by (A.11) and (A.19).

Similarly write $f^{\mathcal{G}^+[k+\Delta k-1,\Delta\ell]}(x) = x_{-d}^{\text{int}} + \hat{h}\zeta_{-d} + \hat{q}$. Let $\hat{h}_1 = \psi(\hat{q})$ and $\hat{x}_1 = x_{-d}^{\text{int}} + \hat{h}_1\zeta_{-d} + \hat{q}$. Then $\hat{x}_1 \in H_{k,\Delta\ell,Q}$, assuming Q is sufficiently large. Let $h_2 = s_{-d}^{\text{step}} + \hat{h}_1\lambda$ and $x_2 = x_{-d}^{\text{int}} + h_2\zeta_{-d} + q$. Then $x_2 \in f^{\mathcal{S}^{(-d)}}(H_{k,\Delta\ell,Q})$ because $x_2 = f^{\mathcal{S}^{(-d)}}(\hat{x}_1)$. Moreover,

$$e_1^\top f^{\mathcal{X}^\top(\mathcal{Y}^\top \mathcal{X})^{\Delta\ell}}(f^{\mathcal{G}^+[k+\Delta k,\Delta\ell]}(x)) = (h - h_2)e_1^\top M_{\mathcal{X}^\top(\mathcal{Y}^\top \mathcal{X})^{\Delta\ell}} \zeta_{-d},$$

thus $h \geq h_2$ by (A.11) and (A.20).

Let $\alpha = \frac{h-h_2}{h_1-h_2}$. Then $f^{\mathcal{G}^+[k+\Delta k,\Delta\ell]}(x) = \alpha x_1 + (1-\alpha)x_2$ and $0 \leq \alpha < 1$, hence $f^{\mathcal{G}^+[k+\Delta k,\Delta\ell]}(x) \in \Phi$.

Step 6. Choose any $x \in \Phi$ and suppose $f^{\mathcal{G}^+[k+\Delta k,\Delta\ell]}(x) \in \Phi$ for some $\Delta k = \mathcal{O}(1)$. To complete the proof it remains to show that $\Delta k = \beta(f^{\mathcal{G}^+[k,\Delta\ell]}(x))$.

Write $f^{\mathcal{G}^+[k+\Delta k,\Delta\ell]}(x) = \alpha x_1 + (1-\alpha)x_2$ where $x_1 \in H_{k,\Delta\ell,Q}$, $x_2 \in f^{\mathcal{S}^{(-d)}}(H_{k,\Delta\ell,Q})$ and $0 \leq \alpha < 1$. Since $x_1 = x_{-d}^{\text{int}} + h_{\Delta\ell}^R \zeta_{-d} + \mathcal{O}(\rho_{\max}^k)$ and $x_2 = x_{-d}^{\text{int}} + h_{\Delta\ell}^L \zeta_{-d} + \mathcal{O}(\rho_{\max}^k)$, we have $x_1 - x_2 = (h_{\Delta\ell}^R - h_{\Delta\ell}^L) \zeta_{-d} + \mathcal{O}(\rho_{\max}^k)$. Thus by (A.11),

$$e_1^\top M_{\mathcal{X}^\top(\mathcal{Y}^\top \mathcal{X})^{\Delta\ell}}(x_1 - x_2) < 0. \quad (\text{A.21})$$

By writing $f^{\mathcal{G}^+[k+\Delta k,\Delta\ell]}(x) = x_1 - (1-\alpha)(x_1 - x_2)$, we obtain

$$e_1^\top M_{\mathcal{X}^\top(\mathcal{Y}^\top \mathcal{X})^{\Delta\ell}}(f^{\mathcal{G}^+[k+\Delta k,\Delta\ell]}(x)) = -(1-\alpha)e_1^\top M_{\mathcal{X}^\top(\mathcal{Y}^\top \mathcal{X})^{\Delta\ell}}(x_1 - x_2), \quad (\text{A.22})$$

which is positive by (A.21). This verifies (A.19). Equation (A.20) can be verified in the same fashion which shows that $\Delta k = \beta(f^{\mathcal{G}^+[k,\Delta\ell]}(x))$ by the definition of β . \square

Proof of Lemma 5.1. By (2.3) and (3.11),

$$u\left(f^{\mathcal{G}^+[k,\Delta\ell]}(v(h))\right) = \omega_{-d}^\top \left(M_{\mathcal{G}^+[k,\Delta\ell]} \left(x_{-d}^{\text{int}} + h\zeta_{-d} \right) + P_{\mathcal{G}^+[k,\Delta\ell]} B - x_{-d}^{\text{int}} \right),$$

thus

$$\frac{d}{dh} u\left(f^{\mathcal{G}^+[k,\Delta\ell]}(v(h))\right) = \omega_{-d}^\top M_{\mathcal{G}^+[k,\Delta\ell]} \zeta_{-d}. \quad (\text{A.23})$$

By (3.4) and (3.16),

$$M_{\mathcal{G}^+[k,\Delta\ell]} = M_{\mathcal{S}^{(-d)}}^{k-\Delta\ell} \zeta_{-d} \omega_{-d}^\top M_{\hat{\mathcal{X}}} M_{\mathcal{S}^{\bar{d}}}^{\Delta\ell} + \mathcal{O}(\rho_{\max}^k). \quad (\text{A.24})$$

Thus using $M_{\mathcal{S}^{(-d)}} \zeta_{-d} = \lambda \zeta_{-d}$ and $\omega_{-d}^\top \zeta_{-d} = 1$ we obtain

$$\frac{d}{dh} u\left(f^{\mathcal{G}^+[k,\Delta\ell]}(v(h))\right) = \lambda^{k-\Delta\ell} \omega_{-d}^\top M_{\hat{\mathcal{X}}} M_{\mathcal{S}^{\bar{d}}}^{\Delta\ell} \zeta_{-d} + \mathcal{O}(\rho_{\max}^k). \quad (\text{A.25})$$

By Lemma 7.1 of [1],

$$\frac{d}{dh} u\left(f^{\mathcal{G}^+[k,\Delta\ell]}(v(h))\right) = \lambda^{k-\Delta\ell} u_0^\top M_{\mathcal{S}^{\bar{d}}}^{\Delta\ell} M_{\hat{\mathcal{X}}} v_0|_{(\eta,\nu)=(0,0)} + \mathcal{O}\left(\frac{1}{k}\right), \quad (\text{A.26})$$

where u_0^\top and v_0 are the left and right eigenvectors of $M_{\mathcal{S}}$ with $u_0^\top v_0 = 1$ and $e_1^\top v_0 = 1$.

In $\Sigma_{k,\Delta\ell}^+$ we have $\lambda^{k-\Delta\ell} = \lambda^k + \mathcal{O}(\frac{1}{k}) = -\tan(\theta) + \mathcal{O}(\frac{1}{k})$ (see equation (A.24) of [1]). Then by the identity $v_{-d} = \frac{-t_d M_{\hat{\mathcal{X}}} v_0}{t_{-d}}$ (Lemma 6.6 of [1]) and the formula for $\kappa_{\Delta\ell}^+$ (B.1), equation (A.26) reduces to (5.2). Equation (5.3) can be derived in a similar fashion. \square

Proof of Theorem 5.2. For brevity we just prove the result in the case $a < 0$.

Step 1. Define $g_{\text{lift,approx}} : [0, 1) \rightarrow \mathbb{R}$ by

$$g_{\text{lift,approx}} := \begin{cases} \varphi \circ u \circ f^{\mathcal{G}^+[k,\Delta\ell]} \circ v \circ \varphi^{-1}, & \text{on } \left[0, \frac{-h_{\Delta\ell}^L}{h_{\Delta\ell}^R - h_{\Delta\ell}^L}\right], \\ \varphi \circ u \circ f^{\mathcal{G}^+[k,\Delta\ell]^{\bar{0}}} \circ v \circ \varphi^{-1}, & \text{on } \left[\frac{-h_{\Delta\ell}^L}{h_{\Delta\ell}^R - h_{\Delta\ell}^L}, 1\right]. \end{cases} \quad (\text{A.27})$$

We first show that

$$g_{\text{lift,approx}} = g_{\text{lift}} + \mathcal{O}\left(\frac{1}{k}\right). \quad (\text{A.28})$$

Both $g_{\text{lift,approx}}$ and g_{lift} are real-valued, piecewise-linear continuous functions on $[0, 1)$ that are comprised of two pieces. The slopes of $g_{\text{lift,approx}}$ are given by (5.2) and (5.3). The slopes of g_{lift} are a_L and a_R (5.6). To show that the leading order components of $g_{\text{lift,approx}}$ and g_{lift} are the same, observe that $\theta_{\Delta\ell}^+ < \theta_{\Delta\ell-1}^+$ because $a < 0$ and $(\kappa_{\Delta\ell}^+ - \kappa_{\Delta\ell-1}^+)a > 0$ by assumption. Thus $\theta_{\min} = \theta_{\Delta\ell}^+$ and $\theta_{\max} = \theta_{\Delta\ell-1}^+$. Then by (B.1), a_L and a_R match (5.2) and (5.3) to leading order. The kink of $g_{\text{lift,approx}}$ is located at $z = \frac{-h_{\Delta\ell}^L}{h_{\Delta\ell}^R - h_{\Delta\ell}^L}$. Using (3.23), (3.24), and $\frac{\nu}{\eta} = \frac{t_{(\ell-1)d}}{t_d} \tan(\theta)$ (2.19), we see that this matches $z_{\text{sw}} = \frac{a_R - 1}{a_R - a_L}$ (the kink of h_{lift}) to leading order. To complete our demonstration of (A.28), we show that the values of $g_{\text{lift,approx}}$ and g_{lift} differ by $\mathcal{O}(\frac{1}{k})$ at their kink points.

The value of g_{lift} at its kink point is

$$g_{\text{lift}}(z_{\text{sw}}) = k^2 \delta + z_{\text{sw}}. \quad (\text{A.29})$$

To evaluate $g_{\text{lift,approx}}$ at $z = \frac{-h_{\Delta\ell}^L}{h_{\Delta\ell}^R - h_{\Delta\ell}^L}$, notice that

$$v\left(\varphi^{-1}\left(\frac{-h_{\Delta\ell}^L}{h_{\Delta\ell}^R - h_{\Delta\ell}^L}\right)\right) = v(0) = x_{-d}^{\text{int}}. \quad (\text{A.30})$$

At any point on the outer boundary of $\Sigma_{k,\Delta\ell}^+$, where $\delta = 0$, we have $\det(P_{\mathcal{G}^+[k,\Delta\ell]}) = 0$. This is because $a < 0$ and is a straight-forward consequence of Theorem 2.4 of [1]. Thus by Lemma 3.6, $f^{\mathcal{G}^+[k,\Delta\ell]}(x_{-d}^{\text{int}}) = x_{-d}^{\text{int}} + \mathcal{O}(\rho_{\text{max}}^k)$ when $\delta = 0$.

At any point on the inner boundary of $\Sigma_{k,\Delta\ell}^+$, where $\delta = \frac{1}{k^2} + \mathcal{O}(\frac{1}{k^3})$ (see §2.4), we similarly have $\det(P_{\mathcal{G}^+[k+1,\Delta\ell]}) = 0$. Thus by Lemma 3.6, $f^{\mathcal{G}^+[k+1,\Delta\ell]}(x_{-d}^{\text{int}}) = x_{-d}^{\text{int}} + \mathcal{O}(\rho_{\text{max}}^k)$. Since $f^{\mathcal{G}^+[k+1,\Delta\ell]} = f^{\mathcal{S}^{(-d)}} \circ f^{\mathcal{G}^+[k,\Delta\ell]}$, by (3.15) we have $f^{\mathcal{G}^+[k,\Delta\ell]}(x_{-d}^{\text{int}}) = x_{-d}^{\text{int}} - s_{-d}^{\text{step}} \zeta_{-d} + \mathcal{O}(\rho_{\text{max}}^k)$, where here $\delta = \frac{1}{k^2} + \mathcal{O}(\frac{1}{k^3})$.

Linear interpolation of these two values of $f^{\mathcal{G}^+[k,\Delta\ell]}(x_{-d}^{\text{int}})$ gives

$$f^{\mathcal{G}^+[k,\Delta\ell]}(x_{-d}^{\text{int}}) = x_{-d}^{\text{int}} - k^2 \delta s_{-d}^{\text{step}} \zeta_{-d} + \mathcal{O}\left(\frac{1}{k^2}\right), \quad (\text{A.31})$$

where the error term can be justified from the smoothness of $f^{\mathcal{G}^+[k,\Delta\ell]}$. Then

$$\varphi\left(u\left(f^{\mathcal{G}^+[k,\Delta\ell]}(x_{-d}^{\text{int}})\right)\right) = \frac{-k^2 \delta s_{-d}^{\text{step}} - h_{\Delta\ell}^L}{h_{\Delta\ell}^R - h_{\Delta\ell}^L} + \mathcal{O}\left(\frac{1}{k}\right), \quad (\text{A.32})$$

and so by (A.13) and (A.30) we obtain

$$g_{\text{lift,approx}}\left(\frac{-h_{\Delta\ell}^L}{h_{\Delta\ell}^R - h_{\Delta\ell}^L}\right) = k^2 \delta - \frac{h_{\Delta\ell}^L}{h_{\Delta\ell}^R - h_{\Delta\ell}^L} + \mathcal{O}\left(\frac{1}{k}\right),$$

matching the value of $g_{\text{lift}}(z_{\text{sw}})$ (A.29) to leading order.

Step 2. Next we derive a formula that is used below to show that $\Delta k = g_{\text{lift}}(z) - g(z)$.

By (3.15), $u\left(f^{\mathcal{S}^{(-d)}}(v(h))\right) = s_{-d}^{\text{step}} + h\lambda$. Using (A.13), since $\lambda = 1 + \mathcal{O}(\frac{1}{k})$, for any $\mathcal{O}(\frac{1}{k})$ value of h we can write

$$u\left(f^{\mathcal{S}^{(-d)}}(v(h))\right) = h_{\Delta\ell}^L - h_{\Delta\ell}^R + h + \mathcal{O}\left(\frac{1}{k^2}\right).$$

Then

$$\varphi\left(u\left(f^{\mathcal{S}^{(-d)}}(v(h))\right)\right) = \varphi(h) - 1 + \mathcal{O}\left(\frac{1}{k}\right).$$

Repeating this result yields the desired formula

$$\varphi(u(T(v(h)))) = \varphi(h) - \Delta k + \mathcal{O}\left(\frac{1}{k}\right), \quad (\text{A.33})$$

where $T = \left(f^{\mathcal{S}^{(-d)}}\right)^{\Delta k}$.

Step 3. Define

$$g_{\text{approx}} := \varphi \circ G \circ \varphi^{-1}, \quad (\text{A.34})$$

where G given by (5.1). Here we show that

$$g_{\text{approx}}(z) = g(z) + \mathcal{O}\left(\frac{1}{k}\right), \quad (\text{A.35})$$

for all $z \in [0, 1) \setminus \Xi_1$, for some set $\Xi_1 \subset [0, 1)$ with $\text{meas}(\Xi_1) = \mathcal{O}(\rho_{\text{max}}^k)$.

By (4.7) and (5.1),

$$g_{\text{approx}} = \begin{cases} \varphi \circ u \circ T \circ f^{\mathcal{G}^+[k, \Delta \ell]} \circ v \circ \varphi^{-1}, & \text{on } \left[0, \frac{-h_{\Delta \ell}^L}{h_{\Delta \ell}^R - h_{\Delta \ell}^L}\right], \\ \varphi \circ u \circ T \circ f^{\mathcal{G}^+[k, \Delta \ell]^{\bar{0}}} \circ v \circ \varphi^{-1}, & \text{on } \left[\frac{-h_{\Delta \ell}^L}{h_{\Delta \ell}^R - h_{\Delta \ell}^L}, 1\right]. \end{cases} \quad (\text{A.36})$$

Since $v(u(x)) = x + \mathcal{O}(\rho_{\text{max}}^k)$ for any x located an $\mathcal{O}(\rho_{\text{max}}^k)$ distance from W^c , we can insert $v \circ u$ into (A.36) to produce

$$g_{\text{approx}} = \begin{cases} \varphi \circ u \circ T \circ v \circ u \circ f^{\mathcal{G}^+[k, \Delta \ell]} \circ v \circ \varphi^{-1} + \mathcal{O}(\rho_{\text{max}}^k), & \text{on } \left[0, \frac{-h_{\Delta \ell}^L}{h_{\Delta \ell}^R - h_{\Delta \ell}^L}\right], \\ \varphi \circ u \circ T \circ v \circ u \circ f^{\mathcal{G}^+[k, \Delta \ell]^{\bar{0}}} \circ v \circ \varphi^{-1} + \mathcal{O}(\rho_{\text{max}}^k), & \text{on } \left[\frac{-h_{\Delta \ell}^L}{h_{\Delta \ell}^R - h_{\Delta \ell}^L}, 1\right]. \end{cases} \quad (\text{A.37})$$

Then by (A.33), $g_{\text{approx}} = g_{\text{lift, approx}} - \Delta k + \mathcal{O}(\frac{1}{k})$, and so by (A.28),

$$g_{\text{approx}} = g_{\text{lift}} - \Delta k + \mathcal{O}\left(\frac{1}{k}\right). \quad (\text{A.38})$$

But $F(v(\varphi^{-1}(z))) \in \Phi$ for all $z \in [0, 1)$. Thus $u(F(v(\varphi^{-1}(z)))) \in [h_{\Delta \ell}^L, h_{\Delta \ell}^R)$ for all $z \in [0, 1) \setminus \Xi_1$, where $\Xi_1 \subset [0, 1)$ contains points near the left and right faces of Φ and $\text{meas}(\Xi_1) = \mathcal{O}(\rho_{\text{max}}^k)$. Thus $g_{\text{approx}}(z) \in [0, 1)$ for all $z \in [0, 1) \setminus \Xi_1$. Therefore $g_{\text{approx}}(z) = g_{\text{lift}}(z) \bmod 1 + \mathcal{O}(\frac{1}{k})$ for all $z \in [0, 1) \setminus \Xi_1$, which verifies (A.35).

Step 4. For any $x \in \Phi$, we have $x - v(u(x)) = \mathcal{O}(\rho_{\text{max}}^k)$. It is straight-forward to show that similarly $F(x) - F(v(u(x))) = \mathcal{O}(\rho_{\text{max}}^k)$ because iterates approach W^c under $f^{\mathcal{S}^{(-d)}}$ and $\lambda^k = \mathcal{O}(1)$. Since $F(v(u(x))) \in \Phi$, we also have $F(v(u(x))) - v(G(u(x))) = \mathcal{O}(\rho_{\text{max}}^k)$. Thus $F(x) - v(G(u(x))) = \mathcal{O}(\rho_{\text{max}}^k)$. Thus by (A.34) and (A.35),

$$F = v \circ \varphi^{-1} \circ g \circ \varphi \circ u + \mathcal{O}\left(\frac{1}{k^2}\right), \quad (\text{A.39})$$

for all $x \in \Phi$ with $z \in [0, 1) \setminus \Xi_1$ where $z = \varphi(u(x))$.

By (A.35) and (A.38), $\Delta k = g_{\text{lift}}(z) - g(z)$ for all but a measure $\mathcal{O}(\frac{1}{k})$ subset of $[0, 1)$ due to the error terms in these expressions. In view of (4.8), equation (5.7) holds unless $z = \varphi(u(x))$ belongs to an $\mathcal{O}(\frac{1}{k})$ subset of $[0, 1)$ where (5.7) is not satisfied due to the $\mathcal{O}(\frac{1}{k})$ difference in the kink points $\frac{-h_{\Delta \ell}^L}{h_{\Delta \ell}^R - h_{\Delta \ell}^L}$ and z_{sw} . \square

B Additional formulas

Suppose (1.2) is at an \mathcal{S} -shrinking point where $\mathcal{S} = \mathcal{F}[\ell, m, n]$. For each $j = 0, (\ell - 1)d, \ell d$ and $-d$ (taken modulo n), let u_j^\top and v_j be the left and right eigenvectors of $M_{\mathcal{S}(j)}$ corresponding to

the eigenvalue 1 and normalised by $u_j^\top v_j = 1$ and $e_1^\top v_j = 1$. Then for all $\Delta\ell \in \mathbb{Z}$, let

$$\kappa_{\Delta\ell}^+ := \begin{cases} u_{\ell d}^\top M_{\mathcal{S}^{\bar{0}(\ell d)}}^{-\Delta\ell-1} v_{(\ell-1)d}, & \Delta\ell \leq -1, \\ u_0^\top M_{\mathcal{S}^{\bar{d}}}^{\Delta\ell} v_{-d}, & \Delta\ell \geq 0, \end{cases} \quad (\text{B.1})$$

$$\kappa_{\Delta\ell}^- := \begin{cases} u_{-d}^\top M_{\mathcal{S}^{\bar{0}}}^{-\Delta\ell} v_0, & \Delta\ell \leq 0, \\ u_{(\ell-1)d}^\top M_{\mathcal{S}^{\bar{d}(\ell d)}}^{\Delta\ell-1} v_{\ell d}, & \Delta\ell \geq 1, \end{cases} \quad (\text{B.2})$$

and assuming $\kappa_{\Delta\ell}^\pm \neq 0$, let

$$\theta_{\Delta\ell}^+ := \begin{cases} \tan^{-1}\left(\frac{t_{(\ell+1)d}}{t_{(\ell-1)d}|\kappa_{\Delta\ell}^+|}\right), & \Delta\ell \leq -1, \\ \tan^{-1}\left(\frac{t_d}{t_{-d}|\kappa_{\Delta\ell}^+|}\right), & \Delta\ell \geq 0, \end{cases} \quad (\text{B.3})$$

$$\theta_{\Delta\ell}^- := \begin{cases} \tan^{-1}\left(\frac{t_d|\kappa_{\Delta\ell}^-|}{t_{-d}}\right), & \Delta\ell \leq 0, \\ \tan^{-1}\left(\frac{t_{(\ell+1)d}|\kappa_{\Delta\ell}^-|}{t_{(\ell-1)d}}\right), & \Delta\ell \geq 1, \end{cases} \quad (\text{B.4})$$

where $\theta_{\Delta\ell}^+ \in (\frac{3\pi}{2}, 2\pi)$ and $\theta_{\Delta\ell}^- \in (\frac{\pi}{2}, \pi)$ if $a < 0$, and $\theta_{\Delta\ell}^+ \in (\frac{\pi}{2}, \pi)$ and $\theta_{\Delta\ell}^- \in (\frac{3\pi}{2}, 2\pi)$ if $a > 0$.

Acknowledgements

The author thanks James Meiss and Chris Tuffley for invaluable discussions regarding homotopies.

References

- [1] D.J.W. Simpson. The structure of mode-locking regions of piecewise-linear continuous maps: I. Nearby mode-locking regions and shrinking points. *Nonlinearity*, 30:382–444, 2017.
- [2] M. di Bernardo, C.J. Budd, A.R. Champneys, and P. Kowalczyk. *Piecewise-smooth Dynamical Systems. Theory and Applications*. Springer-Verlag, New York, 2008.
- [3] D.J.W. Simpson. Border-collision bifurcations in \mathbb{R}^n . *SIAM Rev.*, 58(2):177–226, 2016.
- [4] P.H.E. Tiesinga. Precision and reliability of periodically and quasiperiodically driven integrate-and-fire neurons. *Phys. Rev. E*, 65(4):041913, 2002.
- [5] M. di Bernardo, P. Kowalczyk, and A. Nordmark. Sliding bifurcations: A novel mechanism for the sudden onset of chaos in dry friction oscillators. *Int. J. Bifurcation Chaos*, 13(10):2935–2948, 2003.
- [6] P. Kowalczyk and P.T. Piiroinen. Two-parameter sliding bifurcations of periodic solutions in a dry-friction oscillator. *Phys. D*, 237:1053–1073, 2008.
- [7] M. di Bernardo, C.J. Budd, and A.R. Champneys. Grazing, skipping and sliding: Analysis of the non-smooth dynamics of the DC/DC buck converter. *Nonlinearity*, 11:859–890, 1998.

- [8] Z.T. Zhusubaliyev and E. Mosekilde. *Bifurcations and Chaos in Piecewise-Smooth Dynamical Systems*. World Scientific, Singapore, 2003.
- [9] T. Puu and I. Sushko, editors. *Business Cycle Dynamics: Models and Tools*. Springer-Verlag, New York, 2006.
- [10] M. di Bernardo. Normal forms of border collision in high dimensional non-smooth maps. In *Proceedings IEEE ISCAS, Bangkok, Thailand*, volume 3, pages 76–79, 2003.
- [11] I. Sushko, L. Gardini, and T. Puu. Tongues of periodicity in a family of two-dimensional discontinuous maps of real Möbius type. *Chaos Solitons Fractals*, 21:403–412, 2004.
- [12] J. Laugesen and E. Mosekilde. Border-collision bifurcations in a dynamic management game. *Comput. Oper. Res.*, 33:464–478, 2006.
- [13] Z.T. Zhusubaliyev and E. Mosekilde. Equilibrium-torus bifurcation in nonsmooth systems. *Phys. D*, 237:930–936, 2008.
- [14] R. Szalai and H.M. Osinga. Arnol’d tongues arising from a grazing-sliding bifurcation. *SIAM J. Appl. Dyn. Sys.*, 8(4):1434–1461, 2009.
- [15] D.J.W. Simpson and J.D. Meiss. Shrinking point bifurcations of resonance tongues for piecewise-smooth, continuous maps. *Nonlinearity*, 22(5):1123–1144, 2009.
- [16] W.-M. Yang and B.-L. Hao. How the Arnol’d tongues become sausages in a piecewise linear circle map. *Comm. Theoret. Phys.*, 8:1–15, 1987.
- [17] D.K. Campbell, R. Galeeva, C. Tresser, and D.J. Uherka. Piecewise linear models for the quasiperiodic transition to chaos. *Chaos*, 6(2):121–154, 1996.
- [18] D.J.W. Simpson. *Bifurcations in Piecewise-Smooth Continuous Systems.*, volume 70 of *Nonlinear Science*. World Scientific, Singapore, 2010.
- [19] D.J.W. Simpson and J.D. Meiss. Resonance near border-collision bifurcations in piecewise-smooth, continuous maps. *Nonlinearity*, 23(12):3091–3118, 2010.
- [20] Z.T. Zhusubaliyev, E. Mosekilde, S. Maity, S. Mohanan, and S. Banerjee. Border collision route to quasiperiodicity: Numerical investigation and experimental confirmation. *Chaos*, 16(2):023122, 2006.
- [21] M. di Bernardo, P. Kowalczyk, and A. Nordmark. Bifurcations of dynamical systems with sliding: Derivation of normal-form mappings. *Phys. D*, 170:175–205, 2002.
- [22] M. Arkowitz. *Introduction to Homotopy Theory*. Springer, New York, 2011.
- [23] G.E. Bredon. *Topology and Geometry.*, volume 139 of *Graduate Texts in Mathematics*. Springer, New York, 1993.
- [24] D.J.W. Simpson and J.D. Meiss. Neimark-Sacker bifurcations in planar, piecewise-smooth, continuous maps. *SIAM J. Appl. Dyn. Sys.*, 7(3):795–824, 2008.